ENCLOSURE 2

MFN 06-211

Compilation of GE Responses to RAIs Related to NEDE-33173P

Non-Proprietary Version

IMPORTANT NOTICE

This is a non-proprietary version of Enclosure 1 to MFN 06-211, as well as Attachment 1 to Enclosure 1, which has the proprietary information removed. Portions of the enclosure that have been removed are indicated by an open and closed bracket as shown here [[ ]].

Table of Contents

Table of Tables

Table of Figures

NRC RAI 1.0 Linear Heat Generation Rate (LHGR)
NRC RAI 1.1
Different pins peak at different exposures and in some lattices exhibit high power peaking later in life. Therefore, it is important to assess the overall operating LHGR in these pins relative to the LHGR limit and to understand the available margins such pins have in terms of internal rod pressures. In addition, operating plants data indicates that peak rods could be operating at the limit. Provide internal rod pressure calculations for rods that are operating at the limit for different exposures, including late in the fuel life. Use representative bundles that have lower Gd loading (e.g., 6% or lower).

1. Provide a Minimum LHGR (MLHGR) scatter plots for extended power uprate (EPU) plant.

2. Select most limiting MLHGR at different exposures, including late in the fuel life.

3. Calculate the internal pressure (P) based history for once, twice, and thrice burned fuel near LHR limit and placed on limit for reasonable duration. Compare and discuss the results and exposures.

Response
[[

]]

To respond to RAI 1.1, Brunswick 1 uprated Cycle 15 has been evaluated in detail. The bundles analyzed represent the actual GE14 bundles operated during Brunswick 1 Cycle 15 and reflect six different bundle types; [[

]]

The red diamonds shown in Figure 1.1-2 are the specific cases selected for fuel rod internal pressure evaluation. [[

]]

Table 1.1-1 Fuel Rod Internal Pressure Comparison

[[

]]

[[

]]

Figure 1.1-1 Comparison of Pre-EPU and EPU MLHGR Operating Conditions

[[

]]

Figure 1.1-2 Brunswick 1 Uprated Cycle 15 MLHGR Characterization

NRC RAI 1.2

For Gadolinia (Gd) bearing rod (6 percent) near beginning-of-life (0 to 5.392 gigawatt-days per short ton (GWD/ST)), the LHGR limit increased from 5.392 GWd/STU when the Gd concentration is high to 12.55 GWd/ST at 5 GWD/ST. The Gd rods will be operating at lower powers and the limit is low when the Gd concentration is high. However, it appears that the plant monitoring systems are based on 12.55 GWD/ST. Explain the discrepancies. State why the limit is reduced at low exposures for the Gd loaded pins, when the Gd concentration is high. Discuss under transient conditions if the Gd pin margin to the melting temperature will be much lower?

GE Response

Figure 1.2-1 presents the standard design and licensing analysis basis GE14 6 w/o Gd_2O_3-UO_2 fuel rod peak pellet LHGR vs. exposure power history as compared to the corresponding LHGR operating limit applied in the plant monitoring system. [[

]]

At low exposures, the presence of the high neutron absorption cross-section gadolinium isotopes causes significant neutron flux suppression and a correspondingly low gadolinia fuel rod linear heat generation rate (LHGR). With continued irradiation, the high neutron absorption cross-section gadolinium isotopes progressively transmute to lower neutron absorption cross-section isotopes thereby resulting in a progressive increase in gadolinia fuel rod LHGR. [[

]]

Table 1.2-1 Effect of Early Life LHGR Variation GE14 6 w/o Gd_2O_3-UO_2

[[

]]

[[

]]

Figure 1.2-1 GE14 6 w/o Gd_2O_3-UO_2 LHGR Operating Limit and Analysis Basis

[[

]]

Figure 1.2-2 Comparison of Analyzed and Predicted 6 w/o Gd_2O_3-UO_2 Power Ascension

[[

]]

Figure 1.2-3 GE14 6 w/o Gd_2O_3-UO_2 LHGR Operating Limit and Biased History

NRC RAI 1.3

Fuel failure due to fuel duty is precluded by limiting the initial steady state operating kilowatt per foot (kw/ft) through the LHGR limit. Show that thermal-mechanical fuel duty benchmark data is applicable to EPU conditions.

GE Response

[[

]]

Qualification of the GNF fuel rod thermal-mechanical performance model (GESTR-Mechanical) was performed in a manner to challenge the prediction capability over a wide range of not only duty conditions, but also dimensional conditions and fabrication parameters, to confirm the robustness of the embodied fundamental physical process and mechanism representations. [[

]]

The results of the GESTR-Mechanical experimental qualification have been previously provided to the USNRC (e.g., Reference 1.3-1 and 1.3-2). [[

]]

Regardless, the GNF fuel rod thermal-mechanical performance model (GESTR-Mechanical) has been extensively qualified to pertinent available fuel rod thermal and mechanical performance measurements that extend well beyond extended power uprate conditions, as shown in Table 1.3-1. On this basis, it is concluded that GESTR-Mechanical remains equally applicable to extended power uprate conditions.

References

1.3-1 J. S. Charnley, letter to R. Lobel, "Fuel Property and Performance Model Revisions", MFN-170-84, December 14, 1984.

1.3-2 J. S. Charnley, letter to G. C. Lainas, "Fuel Property and Performance Model Revisions", MFN-027-086, April 7, 1986.

Table 1.3-1 GESTR-Mechanical Qualification Database

[[

]]

[[

]]

Figure 1.3-1 GESTR-Mechanical Fuel Temperature Qualification

[[

]]

Figure 1.3-2 Predicted/Measured Fuel Temperature as a Function of Exposure

[[

]]

Figure 1.3-3GESTR-Mechanical Cladding Diametral Deformation Qualification

[[

]]

Figure 1.3-4 Predicted – Measured Cladding Diametral Deformation vs. Exposure

NRC RAI 1.4
Describe the internal rod pressure validation data that are currently available for both GE fuel designs and legacy fuels.

GE Response
The fuel rod internal pressure is given by

$$P = \frac{nRT}{V}$$

where P = fuel rod internal pressure (psia)
n = gas content occupying the fuel rod void space (gm-moles)
R = universal gas constant
T = temperature of the gases occupying the fuel rod void volume (^{o}R)
V = fuel rod void volume (in^3)

The gas constituents are comprised of the fuel rod initial helium fill gas and released fission gases. [[

]]

Qualification of the prediction capability for the [[ ]] fission gas release component (isotopes of krypton and xenon) has been performed by comparison of predictions to fission gas release measurements [[

]]

[[

]]

The GE14 fuel rod thermal-mechanical analyses, including the fuel rod internal pressure calculation, has been performed with the GESTR-Mechanical model and associated application methodology. These analyses represent the design and licensing basis for GE14. [[

]]

[[

]]

Figure 1.4-1 GESTR-Mechanical Helium Release Comparison

[[

]]

Figure 1.4-2 GESTR-Mechanical Fission Gas Release Qualification

[[

]]

Figure 1.4-3 Predicted – Measured FGR vs. Exposure (Measured FGR < 5%)

[[

]]

Figure 1.4-4 Predicted/Measured FGR vs. Exposure (Measured FGR > 5%)

[[

]]

Figure 1.4-5GESTR-Mechanical Fuel Rod Internal Pressure Qualification

[[

]]

Figure 1.4-6 Predicted – Measured Fuel Rod Internal Pressure vs. Exposure

NRC RAI 2.0 Shutdown Margin (SDM)
Section 2.3 addresses the adequacy of the 0.0038 Δk/k in the calculation of SDM.

NRC RAI 2.1
The demonstration of the shutdown margin is dependent on the cold critical measurement performed at the plant and the eigenvalue for the core with all rods inserted, but with the strongest rod out (Ksro). The code critical measurements are performed after each outage and can be used to demonstrate the adequacy of the neutronics methods for this "distributed" criticality. However, the Ksro value requires experiments to be performed with single rods out, which represent "local" criticality experiments. These local experiments are not performed very frequently, yet the prediction of the SDM relies on the accurate calculation of the Ksro value. The data provided does not distinguish between local cold critical and in-sequence cold critical measurements.

(a) Local cold critical measurements are a more physical demonstration of the stuck rod out (SRO) condition enforced by the 0.0038 Δk/k technical specification limit. Please separate out this data and provide an assessment of the methods accuracy for prediction of the local critical states demonstrating that the bias and uncertainties that are currently applied are adequate for expanded operating domains.

(b) As in Figure 2-5, provide the predicted (e.g., design basis) and measured eigenvalues. Compare the performance versus the distributed cold critical measurements and discuss any other biases or uncertainties that are applied to the Ksro values in the SDM demonstration.

GE Response:
Of the plant data provided in Figure 2-5 of Reference 2-1, plant C contains both in-sequence (distributed) and local cold critical demonstrations. The following Table 2.1-1 includes the local critical data of the figures, plus additional information from prior cycles for plant C. Table 2.1-1 includes both the demonstrated cold critical eigenvalue and the Nuclear Design Basis (NDB) reference eigenvalue for cold shutdown margin and local critical experiments.

The design basis eigenvalue includes [[

]] By comparison with the data reported in Reference 2-1 which indicates that the standard deviation of all differences (both local and distributed) is [[ ]], one may conclude that the predictive performance for local criticals is essentially the same. Additionally, the procedure to [[

]] is effective. This performance again supports the margin discussion contained in Reference 2-1.

Finally, one must note that this database of local critical data for plant C is applicable to other plants primarily because the localized nature of the experiment, which consists of only a small number of withdrawn or partially withdrawn control blades, isolates the event to a very small portion of the core. So, the predictive accuracy for a local critical experiment in any core is readily transferable to other plants and cycles. Additional discussion on the insensitivity of cold critical data to power rating or operational strategy is provided in the response to RAI 2.2.

Table 2.1-1 Plant C Local Critical Eigenvalue Performance

Plant C	Cycle	Test Data	NDB	Delta
Local 1	[[			
Local 2				
Local 3				
Local 1				
Local 2				
Local 3				
Local 4				
Local 1				
Local 2				
Local 3				
Local 1				
Local 2				
Local 1				
Local 2				
Local 3				
Local 4				
Local 5				
Local 6				
Local 7				
Local 8				
Local 1				
Local 2				
Local 3				
Local 1				
Local 2				
Local 3				]]

NRC RAI 2.2

The LTR states that the same SDM Technical Specification value used for non-EPU core designs is adequate for EPU and expanded operating domain conditions. Provide the basis as to why cold SDM is not a strong function of the current operating strategies by comparing cold critical data before and after EPU. Include in the discussion the impact of core designs necessary to achieve EPU and maintain extended cycle lengths (e.g., larger batch fractions, higher bundle enrichments and different core loading patterns).

GE Response:

Cold shutdown margin (SDM) calculations by their nature are not directly evaluated at EPU conditions. Being a calculation (and a subsequent demonstration) performed at the most reactive core conditions, it is evaluated in a cold, unvoided, xenon-free state; not at the rated power/flow conditions. However, as noted, changes in core and fuel designs resulting from design requirements needed to support EPU could potentially impact the calculational accuracy of the SDM analysis. Provided below is a brief discussion of the purpose and limitations of the SDM demonstration itself, followed by a brief discussion of the impact of EPU related design changes on SDM calculations.

During the design and licensing of a reload core, SDM is calculated to provide assurance that the reactor can remain subcritical in the most reactive condition with the highest worth control rod fully withdrawn. The plant Technical Specifications (Tech Specs) further require that a SDM demonstration be performed prior to startup after any core reconfiguration (i.e., at the start of a new cycle) to demonstrate that the plant does indeed remain subcritical with the calculated strongest worth control rod fully withdrawn.

Tech Specs typically require a SDM value of 0.38% $\Delta k/k$ be demonstrated. This demonstration requirement has been put in place so that predictive calculations are not the sole basis of this Tech Spec. By doing so, the bulk of the uncertainties associated with the modeling of SDM are minimized. The Tech Spec requirement has been established because the SDM demonstration itself is subject to variations regarding the core and fuel that cannot be reasonably eliminated. Among these are fuel manufacturing tolerances in ^{235}U enrichment, gadolinia enrichment and component dimensionalities; and control blade reactivity uncertainties due to manufacturing tolerances and control blade burnup variations. These demonstration uncertainties are not dependent primarily on calculational methods or rated power level (i.e., EPU versus non-EPU), but on manufacturing and operational variations.

In performing SDM licensing calculations, a design criterion considerably greater than the Tech Spec requirement is imposed so that there will be a high assurance of success when the demonstration is actually performed. This high assurance of success is desirable from both a safety and a commercial standpoint. At GNF, a SDM design criterion of 1% $\Delta k/k$ has always been required.

Given that a demonstration is always required, the inaccuracies associated with the analytical determination of SDM will always have a built-in confirmation; however, the potential impact of EPU designs on SDM calculations is nevertheless expected to be minimal. The primary influence of EPU designs is the consequence that a higher operating power level (at a similar capacity factor) will require that the core produce more energy for a given cycle length. This higher energy requirement necessitates the loading of fuel of higher enrichment and/or a higher batch fraction of fresh fuel. As for batch fraction, there continues to be a variety of cycle lengths supported by GNF as utilities continue to request designs for annual, eighteen month, and two year cycles, with accompanying variations in batch size. This has allowed GNF to gain considerable experience with both small, intermediate and large batch sizes for both high and low power density cores. The cold critical information previously provided demonstrates that the cold critical calculational accuracy of GNF methods has not suffered a degradation with increasing batch size.

As for enrichment (and discharge exposure), discharge exposure is currently constrained to a maximum value of 70 GWd/MT peak pellet exposure. Many of GNF's non-EPU designs already approach this licensing limit. Thus the ability for EPU fuel designs to increase enrichment and discharge exposure is limited by the constraints already imposed on peak exposure (as well as peak pellet ^{235}U enrichment). Given this, bundle designs for EPU applications are expected to be very similar in enrichment and gadolinia content to non-EPU designs. Batch fractions, however, are proportionally greater than pre-EPU designs. Since somewhat larger batch fraction designs do not result in fuel of higher discharge exposure or significantly different isotopic content, these proportionally larger fresh fuel batch fractions are not viewed as increasing the cold reactivity calculational uncertainties. The validity of this conclusion will be confirmed in the beginning-of-cycle SDM demonstration for EPU cores prior to startup of the initial cycle. Further confirmation will occur as subsequent cycles are operated.

As a final demonstration of these concepts, the trending of the cold eigenvalues for a BWR/4 through a 120% EPU transition is provided in Figure 2.2-1. The scale of the data is consistent with that given in Figure 2-4 of NEDC-33173P. There is no identifiable aberration with the trend because of EPU.

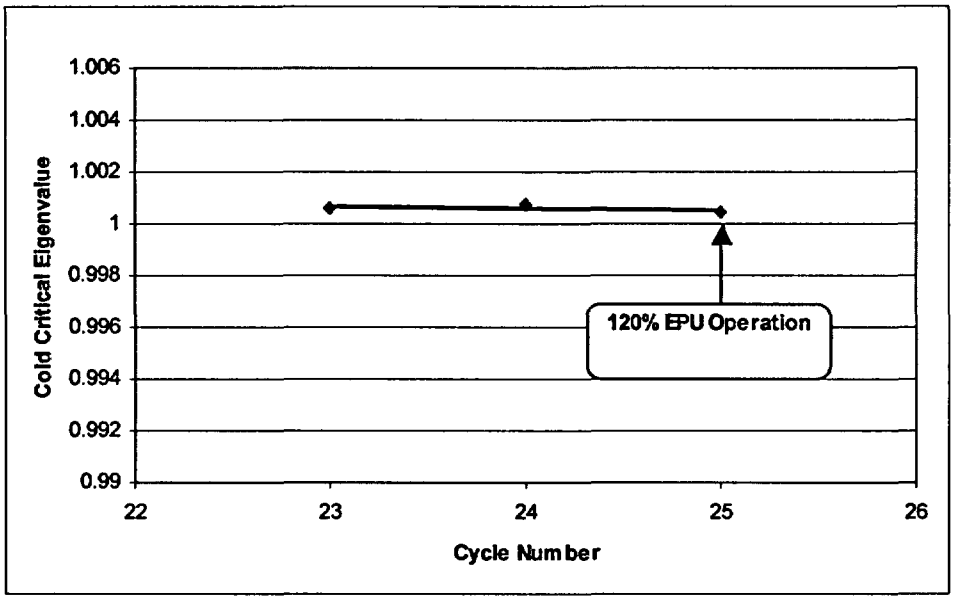

Figure 2.2-1 Sensitivity of Cold Critical Eigenvalue to EPU Operation

NRC RAI 2.3

An equation is provided in Section 2.3.2 stating what the technical specification for cold shutdown requires in terms of ksro and kdemo. Explain the basis for this equation and describe its relationship to the equation relating the SDM calculation to kcrit, ksro, and the period and temperature corrections (e.g., startup control rod withdrawal sequence).

GE Response

The text of interest from Reference 2-1 states the following:

> The cold shutdown technical specification requires that
>
> $$k_{sro} \leq k_{demo}(1. - 0.0038)$$
>
> where k_{sro} is the calculated criticality for the strongest rod withdrawn condition and 0.0038 is the required shutdown margin.

The derivation is different than that provided previously.

$$SDM = k_{crit} - k_{sro} - R + \Delta k_{temp} - \Delta k_{per}$$

Where:
k_{crit} is the multiplication factor for the critical rod pattern;
k_{sro} is the multiplication factor for the strongest rod out;
R is the maximum decrease in SDM throughout the cycle ;
Δk_{temp} is the temperature correction; and
Δk_{per} is the period correction.

The relationship between the two components may be established. SDM at the point in the cycle where the demonstration is performed is

$$SDM = k_{crit} - k_{sro} - R + \Delta k_{temp} - \Delta k_{per,}$$

and the demonstration of plant criticality is

$$k_{demo} = k_{crit} - R + \Delta k_{temp} - \Delta k_{per.}$$

Then,

$$SDM = k_{demo} - k_{sro}$$

$$\frac{SDM}{k_{demo}} = 1 - \frac{k_{sro}}{k_{demo}}$$

Interpreting the SDM requirement as $\frac{\Delta k}{k} \geq 0.0038$, the following must be true:

$$\frac{SDM}{k_{demo}} \geq 0.0038$$

Equating the last two relationships results in the original equation.

$$\frac{SDM}{k_{demo}} = 1 - \frac{k_{sro}}{k_{demo}} \geq 0.0038$$

$$k_{demo} - k_{sro} \geq 0.0038 k_{demo}$$

$$k_{sro} \leq k_{demo}(1 - 0.0038)$$

Considering that $k_{demo} \cong 1$, either interpretation of the SDM requirement is that the strongest rod out is more than 0.38% subcritical.

Reference

2-1 NEDC-33173P "Applicability of GE Methods to Expanded Operating Domains" February 2006.

NRC RAI 3.0 Bypass Voiding

The evaluation of the bypass voiding and its impact on the: (1) neutronic method, (2) effectiveness of the instability protection instrumentation and (3) in-channel thermal-hydraulic conditions are not interim measure in lieu of additional benchmarking data. Instead, the objective of this review is to establish if bypass voiding will yield nonconservative results in the safety analyses and seeks conclusive resolution.

NRC RAI 3.1

(a) Provide a short description of the methodology used to account for the bypass thermal-hydraulic conditions for transient and stability calculations.

(b) Discuss the accuracy of the assumption that the lattice physics parameters can be characterized as a function of the lattice average moderator density. Discuss the impact of bypass and water rod voiding on lattice depletion. Discuss what impact the presence of bypass voiding (E.g., during RPT) not accounted for in the neutronic methods will have on the core thermal-hydraulic conditions (e.g. power distribution). Discuss the effects of bypass and water rod voiding on lattice power distribution for the exposed fuel.

GE Response

Response to Part (a)

The regular cross section generation process creates homogenized cross sections at many depleted and instantaneous conditions. The effects of reduced moderation due to voiding are calculated by performing lattice physic statepoint analysis of different in-channel void conditions. During this process, the out-channel water and water rod are assumed to have the density of saturated water for hot conditions ($>100^{o}C$) and the density of solid sub-cooled water for temperatures $<100^{o}C$.

To accommodate changes in the water rod and bypass water density, the cross sections are then parameterized as a function of node-average relative water density.

$$U=\left(\frac{A_f}{A_f+A_{byp}+A_{wr}}\right)\frac{\rho_f}{\rho_o}+\left(\frac{A_{byp}+A_{wr}}{A_f+A_{byp}+A_{wr}}\right)\frac{\rho_{byp}}{\rho_o}$$

where

ρ_f is the in-channel density with radial (bundle or channel) and axial dependence,

ρ_{byp} is the axially dependent bypass density,

ρ_o is a standard base density,

A_f is the in-channel flow area

A_{byp} is the out-channel (bypass) flow area

A_{wr} is the water rod flow area

and

the subscripts of *f*, *byp* and *wr* indicate the in-channel, bypass, and water rod regions of the lattice.

During the steady-state or kinetics simulator application, the calculated conditions in the bypass, water rod, and active region are combined to calculate the observed node average relative water density and inquire appropriate cross sections.

$$U_{ijk} = \left(\frac{A_f}{A_f + A_{byp} + A_{wr}}\right)\frac{\rho_{ijk}}{\rho_o} + \left(\frac{A_{byp}}{A_f + A_{byp} + A_{wr}}\right)\frac{\rho_{byp,k}}{\rho_o} + \left(\frac{A_{wr}}{A_f + A_{byp} + A_{wr}}\right)\frac{\rho_{wr,k}}{\rho_o}$$

where

$\rho_{f,ijk}$ is the in-channel density with radial (bundle or channel) and axial dependence,

$\rho_{byp,k}$ is the axially dependent bypass density,

$\rho_{wr,k}$ is the axially dependent water rod density for each bundle modeled.

and

A_f is the in-channel flow area

A_{byp} is the out-channel (bypass) flow area

A_{wr} is the water rod flow area

In the 3D simulator PANACEA, the bypass regions and the water rod regions are combined into a single axial nodalized channel for purposes of modeling moderator density. The in-channel, bypass and water rod regions are then combined as described in the equation above to form the nodal average lattice moderator density.

In the plant transient simulator TRACG, the bypass and water rod regions are treated separately and are nodalized in the axial direction as specified by application. The in-channel, bypass and water rod regions are then combined as described in the equation above to form the nodal average lattice moderator density.

Thus, by the use of the lattice average water density parameter, potential changes in the bypass and water rod voiding (water density) are accurately modeled in the core steady-state and transient simulators.

Response to Part (b)

The presence of bypass and water rod voiding is accounted for in the neutronic methods through the process discussed in the response to RAI 3.1(a). The accuracy of the nodal, axial and radial power distribution is directly related to the ability of the 3D simulators to model the nodal reactivity accurately. In the following discussion, it is shown that the nominal impacts for bypass and water rod voids on the axial power distribution are accurately accounted for in the 3-dimensional steady state and transient methods.

In MFN 05-31 RAI 1.4, the adequacy of the polynomial fitting process under high in-channel voids with and without bypass and water rod voiding was addressed using MCNP. The review in MFN 05-31, RAI 1.4 covered the ability to extrapolate to either the 90% in-channel void without water rod and bypass void state or to the 85% in-channel void with 25% water rod and 10% bypass void state. In this RAI, the error in the reactivity (k-infinity) fit extrapolation from the 0,40, and 70% void fraction base data to the 90% void fraction level was shown to be less than 0.7% for the lattice evaluated. The error associated with the presence of bypass and water rod voiding is less than 0.5% and will not contribute to a significant decrease in the ability of the 3D simulators to predict the axial power distributions. Figure 3.1-1is taken from MFN 05-31, RAI 1.4 for completeness.

Additional evaluations of the accuracy of this assumption for the components of k-infinity are provided to support the accuracy of the lattice average moderator assumption. The component cross sections evaluated are macroscopic thermal absorption (capture + fission), macroscopic thermal fission, macroscopic fast to epi-thermal scattering cross section and the epi-thermal to thermal scattering cross section. The calculated flux ratios are also presented to demonstrate the overall effectiveness of this assumption.

To perform this evaluation, a lattice depletion at a 40% void fraction was perform to create the base data for the instantaneous void evaluation using TGBLA. Using the isotopics generated by the base depletion case, the state points identified in Table 3.1-1, Instantaneous Void Evaluation Conditions were evaluated with MCNP. The instantaneous void data is fit as a function of lattice average moderator density at several exposure points from beginning of lattice life to assumed end of lattice life (65 Gwd/st). The base fits are performed by use of the 0, 40, and 70% void fraction data and these fits are then evaluated at lattice average moderator density values equivalent from a 0% in-channel state to a 90% in-channel without bypass or water rod voiding state to provide the fitted data representation in Figure 3.1-2 through Figure 3.1-7. Two explicit MCNP calculations for high voids with and without bypass voiding at each of the 4 exposure points were then performed to provide the basis for the comparison.

From Figure 3.1-2 through Figure 3.1-7, it can be seen that these significant nodal parameters can be fit and extrapolated with a high degree of accuracy and that the presence of bypass and water rod voiding can be parameterized as overall lattice average moderator density with a high degree of accuracy. No noticeable degradation in the nodal evaluations can be attributed to the presence of bypass and water rod void.

Since the nominal operating core does not experience bypass and water rod voiding and that the core conditions with bypass and water rod voiding are transitory in nature, there will be no significant impact on core depletion simulation.

The lattice physic state point analysis assumes non-voided bypass regions and water rods; therefore, the local pin power distributions do not account for the voided bypass and water rod effects. Evaluations for the impact of the non-voided bypass and water rod assumption show that the uncertainty in the local pin power distribution is small and that the subsequent impact on the R-factor process is small.

In the reactor core, the probability that a node experiencing bypass and water rod voiding is a maximum powered node is extremely small. However, to review the impact of bypass and water rod voiding, a comparison was made between a lattice at 90% in-channel voids without bypass and water rod voiding and a lattice at 85% in-channel voids with 10% bypass voids and 25% water rod voids. This combination of in-channel, bypass and water rod voids produces essentially identical average moderator density. To perform this comparison, a upper zone lattice from a bundle designed for MELLLA+ operation was chosen and the isotopics are based on a 70% in-channel void fraction without water rod and bypass void depletion case.

In Figure 3.1-8and Figure 3.1-9, the impact on local pin fission density is presented. In Figure 3.1-8, the normalized fission density peaking is presented for the lattice at 90% in-channel void fraction without water rod and bypass voiding and for the lattice at 85% in-channel void fraction with 25% water rod and 10% bypass voiding. Figure 3.1-9 contains the delta normalized fission density for four (4) fuel pins for which at some point in the lattice lifetime are the peak powered rod. The contiguous rod peaking is plotted to demonstrate the impact as the peak powered rod changes location as a function of lattice exposure.

[[

]]This impact will not impact the accuracy of the LHGR evaluation in the neutronic methods.

From MFN 05-31 RAI 18, the Figure 3.1-10 below shows that the impact of the voiding of the bypass and water rods has a minimal impact on the value of the R-factor. A bundle that was designed for use in a MELLLA+ core design was used for this evaluation. This comparison is made by using the standard "production" three void points (0,40, and 70%)

without bypass and water rod voiding as the base case for the R-factor generation process. The 90VF_axial-4VP model is generated by using four void points at 0, 40, 70, and 90VF without bypass and water rod voiding. The 90VF_20BP-4VF was generated by using 0, 40, and 70 VF without bypass and water rod voiding and a 90 in-channel void with 20% bypass and water rod voiding case for the fourth data point for the R-factor generation process.

As can be seen below, the magnitude of the perturbed R-factor can vary both positive and negative relative to the base "production" R-factor and hence the modeling of bypass and water rod voiding in the R-factor generation process is neither conservative nor non-conservative.

Table 3.1-1 Instantaneous Void Evaluation Conditions

Lattice State	Lattice Exposure (Gwd/st)	In-channel Void (%)	Bypass Void (%)	Water Rod Void (%)
1	0.2,13,65	0	0	0
2	0.2,13,65	40	0	0
3	0.2,13,65	70	0	0
[[				
				]]

[[

]]

Figure 3.1-1 Fit Uncertainty for TGBLA06 Reactivity

[[

]]

Figure 3.1-2 Macroscopic Group 3 (thermal) Sigma Absorption

[[

]]

Figure 3.1-3 Macroscopic Group 3 (thermal) Sigma Fission

[[

]]

Figure 3.1-4 Macroscopic Sigma Slowing Group 1 (Fast) to Group 2 (Epi-thermal)

[[

]]

Figure 3.1-5 Macroscopic Sigma Slowing Group 2 (Epi-thermal) to Group 3 (thermal)

[[

]]

Figure 3.1-6 Group 1 (Fast) to Group 3 (thermal) Flux Ratio

[[

]]

Figure 3.1-7 Group 2 (Epi-thermal) to Group 3 (thermal) Flux Ratio

[[

]]

Figure 3.1-8 Peak Rod Fission Density Impact for Bypass and Water Rod Voiding

[[

]]

Figure 3.1-9 Peak Rod Delta Fission Density for Bypass and Water Rod Voids

[[

]]

Figure 3.1-10 R-factor Response for 20% Bypass/Water Rod Void Fraction (from MFN 05-133 RAI 18)

NRC RAI 3.2
NRC RAI 3.2(a)
Quantify the bypass voiding for rated power operation and power levels associated with EPU and MELLLA+.

(i) Describe the methodologies used by GE to calculate bypass voiding.

(ii) Quantify the best estimate bypass void fraction (BP VF) for the worst point in the operating map (NC + MELLLA+, MELLLA, OLTP) that could be used for stability calculations.

(iii) Quantify the best estimate BP VF for the expected conditions where ODYSY stability methodology is used for LTS.

GE Response:
Response to Part 3.2(a)(i)
The core bypass region modeling used in the various GE codes (ISCOR, PANACEA, ODYSY and TRACG) is described below. A summary comparison table is provided at the end.

ISCOR
ISCOR employs a core-averaged bypass model. [[

]]

PANACEA
PANACEA utilizes a core-averaged bypass model that is consistent with the ISCOR model described above. [[

]] The PANACEA bypass model considers the same sources of heating as the ISCOR model. The core-averaged bypass region uses the same axial nodalization as the PANACEA active channel model. Pressure drop and void correlations used in PANACEA are consistent with the ISCOR correlations.

ODYSY
ODYSY utilizes a core-averaged bypass model that is consistent with the ISCOR model described above. The ISCOR calculated bypass and water rod flow is used as input for the ODYSY calculations. [[

]] The core-averaged bypass region uses the same axial nodalization as the ODYSY active channel model. Pressure drop and void correlations used in ODYSY are consistent with the ISCOR correlations.

TRACG
In TRACG, the bypass region is modeled as [[

]] The two ring nodalization is shown in Figure 3.2(a)-1.

[[

]]

SUMMARY
Table 3.2-1 below summarizes the key elements of the bypass modeling for the various GE codes.

Response to Part 3.2(a)(ii)
TRACG is used to compute the best estimate bypass void fraction for the worst point in the power/flow operating map, i.e. at the intersection of the natural circulation line and the MELLLA+ boundary. [[

]] This is a best estimate value of the bypass voids and the TRACG bypass voiding methodology is described in the response to RAI 3.2a(i).

ISCOR is used to compute bounding values of the bypass void fraction for the worst point in the power/flow operating map, i.e. at the intersection of the natural circulation line and the MELLLA+ boundary, for comparison to the values calculated by TRACG. ISCOR calculations are also performed at the intersection of the natural circulation line and the MELLLA boundary and at the intersection of the natural circulation line and the original licensed thermal power (OLTP) rated rod line to show the sensitivity of bypass voids to power level. ISCOR core average and hot channel bypass voids are shown in Table 3.2-2 and the ISCOR bypass voiding methodology is described in the response to 3.2a(i). ISCOR in-channel voids are also provided in Table 3.2-2 for reference. [[

]]

Therefore, because TRACG computes best estimate bypass voiding and the calculation for the worst point on the power/flow map of [[

]], which has a negligible effect on the effectiveness of the instability protection instrumentation.

Response to Part 3.2(a)(iii)

ODYSY is used to calculate the stability exclusion region for BWROG Long-Term Solution Options I-D and II. The Vermont Yankee Cycle 25 Option I-D exclusion region analysis was reviewed to determine the bypass void fractions computed by ISCOR for the endpoints of the exclusion region boundary. [[

]]

Therefore, bypass voiding has no effect on the ODYSY exclusion region methodology (e.g., application to Options I-D and II).

Table 3.2-1

	ISCOR	PANACEA	ODYSY	TRACG
[[				
				]]

Reference

3.2(a)-1 NEDE-32176P, Revision 3, "TRACG Model Description Licensing Topical Report," April 2006.

Table 3.2-2

[[					

]]

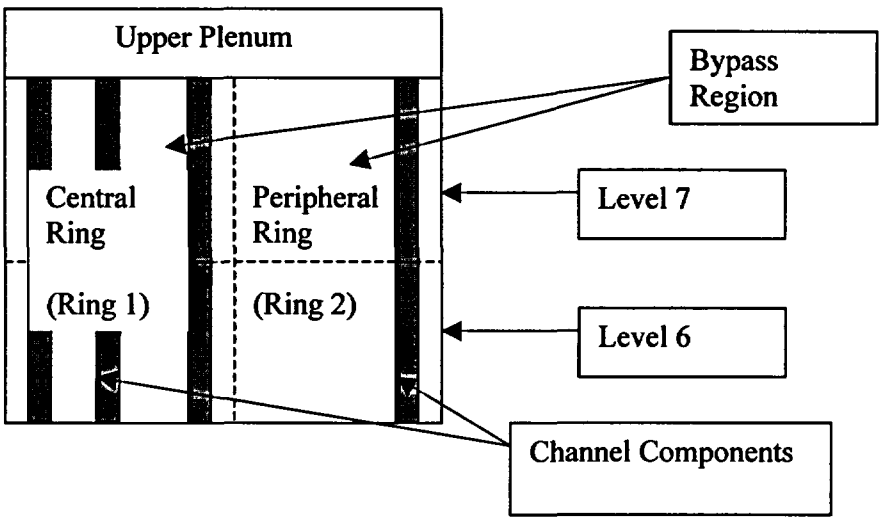
Upper Plenum
Bypass Region
Central Ring
(Ring 1)
Peripheral Ring
(Ring 2)
Level 7
Level 6
Channel Components

Figure 3.2(a)-1

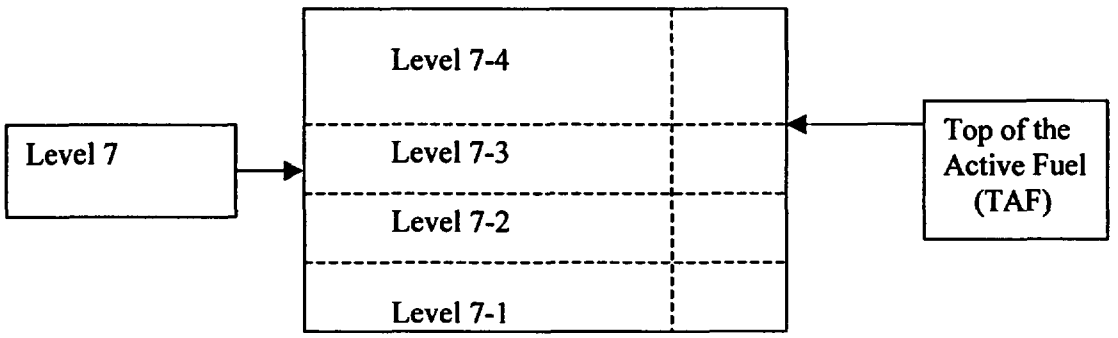
Level 7-4
Level 7
Level 7-3
Top of the Active Fuel (TAF)
Level 7-2
Level 7-1

Figure 3.2(a)-2

NRC RAI 3.2(b)
Describe the method for the determination of the impact of BP VF on stability analysis.

GE Response
Two different approaches are used in GE stability analysis – the frequency-domain code ODYSY and the time-domain code TRACG.

ODYSY employs the conservative estimates for direct moderator heating from ISCOR. [[

]] Therefore, the ODYSY model provides a reasonably bounding value of bypass voiding.

[[

]] Both the regional and core-wide DIVOM analyses are performed at a reasonably limiting power/flow point where bypass voiding tends to be the worst. (The core-wide DIVOM analysis is performed at the rated rod line and the natural circulation line, while the regional DIVOM analysis is performed on the highest flow boundary and natural circulation flow). However, both the regional and core-wide DIVOM analyses are based on the hot channels, which are away from the periphery of the core where bypass voiding is highest. This mitigates the bypass voiding impact on the DIVOM evaluation.

Reference
3.2(b)-1 NEDE-32906P-A, Revision 2, "TRACG Application for Anticipated Operational Occurrences Transient Analyses," February 2006.

NRC RAI 3.2(c)

Section 2.6.2.1 concludes that the effect of BP VF on APRM calibration is [[ ]] Section 2.6.2.3 concludes that the effect of BP VF on OPRM calibration is [[ ]] Please describe the methodology used for these analyses and quantify the BP VF levels used.

GE Response

The APRM evaluation in Section 2.6.2.1 makes use of the core average bypass voids computed by the ISCOR thermal-hydraulics model. This is appropriate because the APRM is a core average response. The OPRM evaluation in Section 2.6.2.3 makes use of the hot channel bypass voids computed by ISCOR. This is appropriate because the OPRM is a localized response. [[

]] The bypass voids used in the analyses and the corresponding in-channel voids are provided in Table 3.2(c)-1. The APRM evaluation data is from Vermont Yankee under EPU/MELLLA conditions. The OPRM evaluation data is from another BWR/4 under EPU/MELLLA conditions.

Table 3.2-1

[[				

]]

NRC RAI 4.0 Use of 40 % Void Fraction History Depletion Assumption for Instantaneous Void Fraction Changes.

The neutonics methods perform void history calculations a 0%, 40%, and 70% void fractions, but the instantaneous branch cases are performed only for the 40% void history case. As a result, the impact of instantaneous changes in the void fraction for all void histories is assumed to be that of the 40% void history case. The impact of this assumption results in errors in the prediction of the void reactivity effect for void fraction histories lower and higher than 40% and can be evaluated by examining the void coefficient of reactivity. In order to assess the impact of the 40% void fraction history assumption:

NRC RAI 4.1
NRC RAI 4.1(a)

Provide an evaluation of the error created by the 40% void fraction history assumption on the local void coefficient.

GE Response

Response to 4.1(a)

As described in Reference 4.1(a)-1 Section 2.2.2.2, the local void coefficient error created by the [[

]]

References

4.1(a)-1 Licensing Topical Report, "Applicability of GE Methods to Expanded Operating Domains," NEDC-33173P, February 2006.

4.1(a)-2 Entergy letter to U.S. Nuclear Regulatory Commission, "Vermont Yankee Nuclear Power Station, License No. DPR-28 (Docket No. 50-271), Technical Specification Proposed Change No. 263 - Supplement No. 35, Extended Power Uprate - Response to Request for Additional Information," BVY 05-088, September 28, 2005.

[[

]]

Figure 4.1a-1 Void Coefficient Ratio MNCP / TGBLA06

NRC RAI 4.1(b)

Provide an estimate of the error in the global void coefficient introduced by the [[ ]] assumption.

GE Response

TRACG was used to estimate the error in the global void coefficient introduced by the [[ ]] assumption. Analysis was performed for a high power density BWR/6 at natural circulation and a high rod line. A TRACG base case was run with the void coefficient correction included. The hot channel power response for this case is shown in Figure 4.1b-1. To estimate the error in the global void coefficient due to the [[ ]] assumption, a second TRACG case was run using an input variable to increase the global void coefficient. It was determined that [[ ]] in the global void coefficient yields results that closely match the results with the void coefficient correction included. The hot channel power response for the second case is shown in Figure 4.1b-2. Therefore, the error in the global void coefficient introduced by the [[ ]] assumption is [[ ]].

[[

]]

Reference

4.1(b)-1 Licensing Topical Report, "ODYSY Application for Stability Licensing Calculations," NEDC-32992P-A, July 2001.

4.1(b)-2 Licensing Topical Report, "Reactor Stability Detect and Suppress Solutions Licensing Basis Methodology for Reload Applications," NEDO-32465-A, August 1996.

[[

]]

Figure 4.1b-1 Hot Channel Power Response with Void Coefficient Correction

[[

]]

Figure 4.1b-2 Hot Channel Power Response with [[ ]] Increase in Global Void Coefficient

NRC RAI 4.1(c)
Provide TRACG stability calculations with and without the void history correction for void coefficient.

GE Response
TRACG analysis was performed for a high power density BWR/6 at natural circulation and a high rod line. Figure 4.1c-1 shows the hot channel power and growth rate with and without the void history correction for the void coefficient. The data with the correction is labeled "V33" and the data without the correction is labeled "NV". As can be seen in Figure 4.1(c)-1, the correction produces [[

]].

[[

]]

Figure 4.1c-1 Hot Channel Power and Growth Rate with (V33) and without (NV) Void History Correction for Void Coefficient

NRC RAI 4.1(d)
Provide and include the cited instability benchmarking that demonstrates the accuracy of ODYSY and TRACG in the TR. Provide some assessment of the similarities of core thermal-hydraulic conditions between the benchmark plants and the EPU plants.

GE Response:
ODYSY
ODYSY stability benchmarking is provided in References 4.1(d)-1 and 2. Reference 4.1(d)-1 provides a comparison of ODYSY calculated decay ratios to plant data for core-wide mode oscillations from Vermont Yankee high decay ratio tests and the 1988 LaSalle instability event. These data are shown in Tables 4.1d-1 and 4.1d-2, respectively. It can be seen from the data that the ODYSY calculated decay ratios are in good agreement with the test data. The ODYSY predicted frequency is slightly lower than the test data.

Reference 4.1(d)-1 also provides ODYSY predicted core and limiting channel decay ratios for regional mode oscillations from tests at Leibstadt and KRB-C and the 1991 Cofrentes instability event. The ODYSY results are compared to the ODYSY stability criteria map in Figure 4.1d-1. Regional mode oscillations are possible when the limiting channel decay ratio exceeds the curved line that begins at 0.56. As can be seen in Figure 4.1d-1, the ODYSY predicted core and limiting channel decay ratios for the tests and instability event exceed the stability criteria. Therefore, the combination of the ODYSY calculated decay ratios and the ODYSY stability criteria map provide a good prediction for regional mode oscillations.

Also provided in Reference 4.1(d)-1 is a comparison of ODYSY predicted channel decay ratio versus TRACG predicted channel decay ratio for selected channels from Leibstadt and LaSalle. This comparison is shown in Figure 4.1d-2. As can be seen in Figure 4.1d-2, the ODYSY calculated channel decay ratios are in good agreement with the TRACG calculated channel decay ratios.

Reference 4.1(d)-2 provides a qualification study of the 1995 Laguna Verde instability event. The ODYSY calculated core and limiting channel decay ratios at instability inception for different power and xenon assumptions are provided in Table 4.1d-3. Condition 3c is believed to be the most accurate calculation. The actual event produced a limit cycle oscillation, so the actual core decay ratio was exactly 1.0 when the oscillation was fully developed. The ODYSY predicted core decay ratio is in good agreement with the actual decay ratio.

The ODYSY predicted core and limiting channel decay ratios for the 2003 Nine Mile Point 2 (NMP-2) instability event versus the ODYSY stability criteria are shown in Figure 4.1d-3. Two conditions were analyzed. The first calculation was performed at the Average Power Range Monitor (APRM) measured power of 44.9%, a measured core flow of 28%, and a measured feedwater temperature of 360 °F. The second calculation was performed at a predicted power of 47.1%, the measured core flow of 28%, and the

measured feedwater temperature of 360 °F. The 47.1% power was based on a GE 3D BWR core simulator prediction for the measured core flow, feedwater temperature, and rated power and flow eigenvalue. It is believed that the predicted core power of 47.1% is more accurate for the event. As can be seen in Figure 4.1d-3, the ODYSY prediction for the 47.1% power case is greater than the ODYSY stability criteria, indicating that core-wide mode oscillations are possible.

The ODYSY predicted core and limiting channel decay ratios for the 2005 Perry instability event versus the ODYSY stability criteria are shown in Figure 4.1d-4. Four conditions were analyzed corresponding to the progression of the feedwater temperature from the rated condition to the equilibrium condition. It is believed that the case with the equilibrium feedwater temperature of 372 °F is believed to be the most accurate calculation. As can be seen in Figure 4.1d-4, the ODYSY prediction for the 372 °F feedwater temperature case is greater than the ODYSY stability criteria, indicating that core-wide mode oscillations are possible.

ODYSY has been qualified to a very broad range of conditions and events. The ODYSY predicted results have universally shown good agreement to plant data and ODYSY is believed to be a very good tool for predicting and evaluating core and channel decay ratios for both core-wide and regional mode oscillations.

TRACG
TRACG stability benchmarking is provided in the TRACG qualification report (NEDE-32177P, Reference 4.1(d)-3). Simulations of the instability events at LaSalle and Cofrentes and the stability tests at Leibstadt and Forsmark are presented.

The 1988 LaSalle event provides an assessment of the prediction of core-wide mode oscillations. TRACG successfully calculated the core-wide oscillations observed during the event. The characteristics of the oscillations and sensitivity to the feedwater flow fluctuations were well predicted. The prediction of the reactor transient response following the pump trip was also well predicted. Figures 4.1d-9 and 10 (Figures 7.4-10 and 7.4-11 from Reference 4.1(d)-3) are included below.

The 1991 Cofrentes event provides an assessment of the regional oscillation mode predictive capability of TRACG. Reasonable agreement between TRACG and the event data for APRM frequency and magnitude was obtained. The TRACG analysis of the event demonstrates that the oscillations were out-of-phase and that operator action reduced the effect of the out-of-phase oscillation. Figures 4.1.d-11 and 12 (Figures 7.7-7 and 7.7-8 from Reference 4.1(d)-3) are included below.

The Leibstadt stability tests provide data to assess the prediction of regional oscillation characteristics. TRACG successfully calculated the limit cycle regional oscillations observed during the tests. The characteristics of the oscillations and sensitivity to changes in test conditions were well predicted. Tables 4.1d-7 and 8 (Tables 7.5-1 and 7.5-2 from Reference 4.1(d)-3) are included below.

The Forsmark stability tests provide data for the assessment of TRACG to calculate core decay ratios for an internal pump plant. The TRACG model of Forsmark Unit 1 was validated against plant data. The TRACG calculated and measured decay ratios correspond well for the five tests considered. At the limit cycle condition, TRACG predicts the limit cycle oscillation. Tables 4.1d-6 and 7 (Figures 7.6-1 and 7.6-3 from Reference 4.1(d)-3) are included below.

A TRACG benchmark calculation was performed for the recent NMP-2 instability event and the result is shown in Figure 4.1d-5. The figure presents a comparison of the TRACG calculated Oscillation Power Range Monitor (OPRM) cell signal to the plant OPRM cell signal just prior to the reactor scram. It can be seen from the figure that the oscillation frequency and growth rate are well predicted.

Analysis was performed relative to the NMP-2 Instability TRACG benchmark to show the sensitivity of the oscillation response to core flow, power and feedwater temperature. The flow sensitivity is shown in Figure 4.1d-6. It can be seen from the figure that the oscillation growth rate is very sensitive to the core flow, while the frequency has a small sensitivity. The power sensitivity is shown in Figure 4.1d-7. It can be seen from the figure that the oscillation growth rate is not as sensitive to power as core flow. The frequency is not affected. The feedwater temperature sensitivity is shown in Figure 4.1d-8. It can be seen from the figure that the oscillation growth rate is very sensitive to the feedwater temperature, while the frequency has a small sensitivity.

Core Thermal-Hydraulic Conditions

The ISCOR core average and hot channel in-channel voids for the benchmark NMP-2 and Perry instability events and the VY and Hope Creek EPU/MELLLA conditions are provided in the Table 4.1d-4. The NMP-2 and Perry instability events occurred very near natural circulation at a high rodline. The VY and Hope Creek data is shown for natural circulation at the MELLLA rodline. It can be seen from the data that the in-channel voids for the benchmark plants are very close to the in-channel voids for the EPU plants. Therefore, it can be concluded that the validation database adequately covers the EPU plants.

References

4.1d-1 NEDC-32339P-A, "Reactor Stability Long-Term Solution: Enhanced Option I-A, ODYSY Application to E1A," December 1996.
4.1d-2 NEDC-32992P-A, "ODYSY Application for Stability Licensing Calculations," July 2001.
4.1d-3 NEDE-32177P, Rev. 2, "TRACG Qualification," January 2000.

Table 4.1d-1 Summary of ODYSY Results for Vermont Yankee High Decay Ratio Tests

Test Point	Power/Flow (% rated)	Test Data		ODYSY Results	
		Decay Ratio	Frequency	Decay Ratio	Frequency
6P	57.2/38.5	0.74	0.44	0.67	0.39
7N	51.2/32.6	1.00	0.43	0.99	0.38
8P	50.9/32.6	0.96	0.43	0.97	0.37
9P	48.1/32.4	0.81	0.42	0.86	0.36
10P	49.8/33.0	0.90	0.42	0.97	0.37
11P	67.1/38.5	0.85	0.47	0.85	0.42
12P	63.1/38.5	0.78	0.47	0.75	0.42

Table 4.1d-2 Summary of ODYSY Results for LaSalle Event

Condition	Power/Flow (% rated)	Event Data		ODYSY Results	
		Decay Ratio	Frequency	Decay Ratio	Frequency
17:35 Threshold	42/28	1.00	0.45	1.00	0.40
17:37 At Scram	45/28	Unstable >1.00	0.45	1.18	0.44

Table 4.1d-3 Summary of ODYSY Results for Laguna Verde Event

Condition	Description	Xenon Assumption	Core Decay Ratio	Channel Decay Ratio
3a	After flow control valve closure at initiation of reactor instability, 31.8% power, 32% core flow	Constant xenon at 16% power	0.89	0.48
3b	Repeat of Case 3a with transient xenon model	Transient xenon model	0.94	0.50
3c	Repeat of Case 3a with transient xenon model and at 33.1% power	Transient xenon model	1.04	0.54

Table 4.1d-4 ISCOR In-Channel Voids for Selected Events and Conditions

Event/Condition	ISCOR Core Average In-Channel Voids (Top of Active Fuel)	ISCOR Hot Channel In-Channel Voids (Top of Active Fuel)
NMP-2 Instability Event	73%	81%
Perry Instability Event	75%	86%
VY EPU/MELLLA	76%	85%
Hope Creek EPU/MELLLA	76%	86%

Table 4.1d-5 (NEDE-32177P Rev 2 Table 7.5-1) Leibstadt Test Conditions

Test	Power (MW)	Flow (kg/s)	Dome Pressure (MPa)	Feedwater Temperature (K)
4	1646	3434	6.736	448
4A	1599	3211	6.736	448
5	1528	3434	6.698	434
5A	1392	3234	6.698	434

Table 4.1d-6 (NEDE-32177P Rev 2 Table 7.5-2) Leibstadt Test Data TRACG Comparison Summary

Test	LPRM (%)*		APRM (%)*		Freq (Hz)	
	Data	TRACG	Data	TRACG	Data	TRACG
4	14	20	4	2	0.45	0.41
4A	66	26	8	3	0.45	0.39
5	12	19	4	2	0.45	0.41
5A	12	13	4	2	0.45	0.39

* (P – P)/A

Table 4.1d-7 (NEDE-32177P Rev 2 Table 7.6-1) Forsmark Test Conditions

Test	5	7	8	15
Power (% of 2800 MW)	62.7	73.4	70.0	103.5
Flow (kg/s)	4205	4797	4530	10166.
CR Position (–10000 notches)	128	272	324	634
Xe (t/cm)	870	809	833	1311

Table 4.1d-8 (NEDE-32177P Rev 2 Table 7.6-3) Forsmark Decay Ratio Comparison

Test	5	7	8	15
DR	0.84	0.86	0.96	0.05
Data Freq (Hz)	0.51	0.55	0.54	
DR	0.77	0.97	1.03	<0.20
TRACG Freq (Hz)	0.55	0.61	0.60	

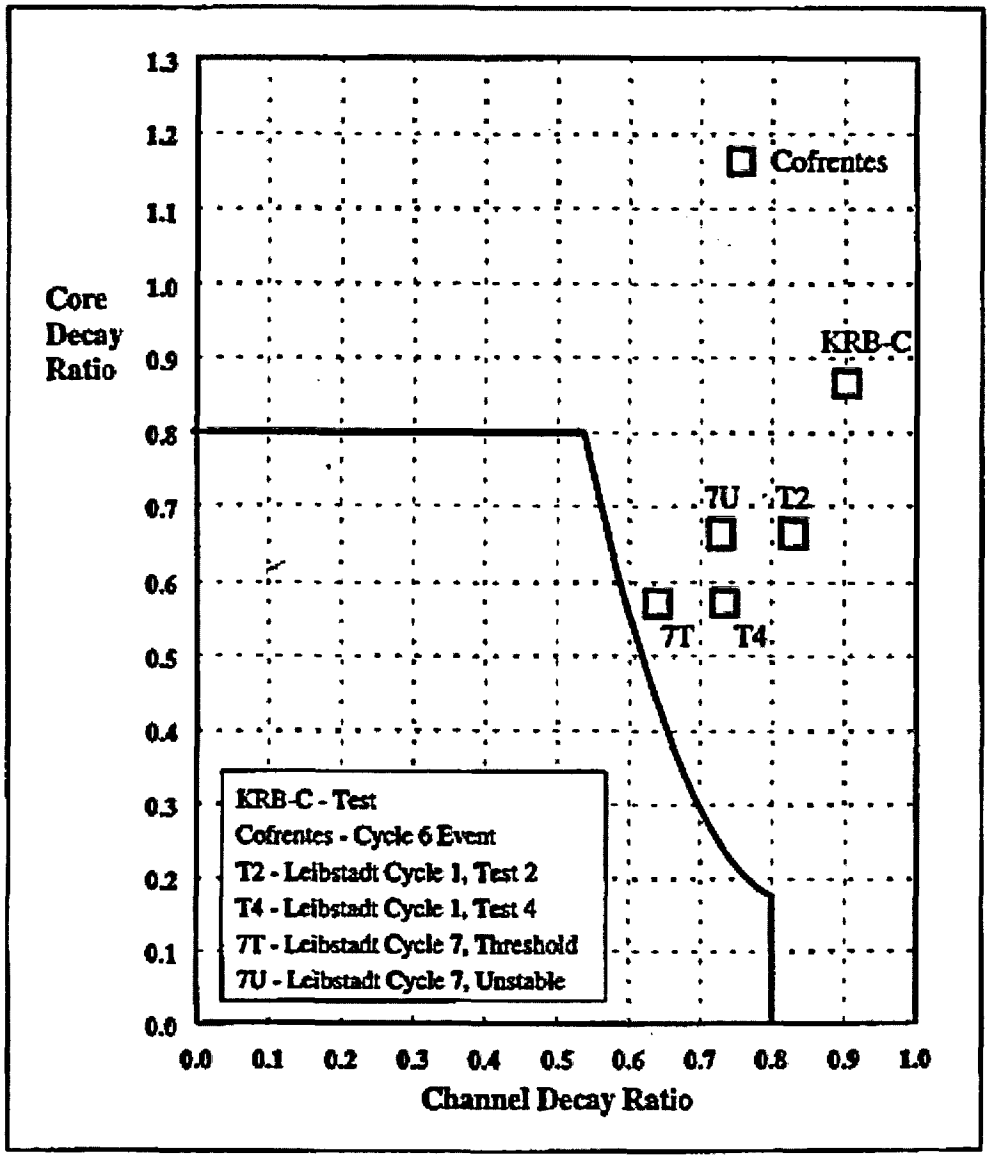

Figure 4.1d-1 Regional Mode Instability Event and Test Decay Ratios: ODYSY Results vs. ODYSY Stability Criteria Map

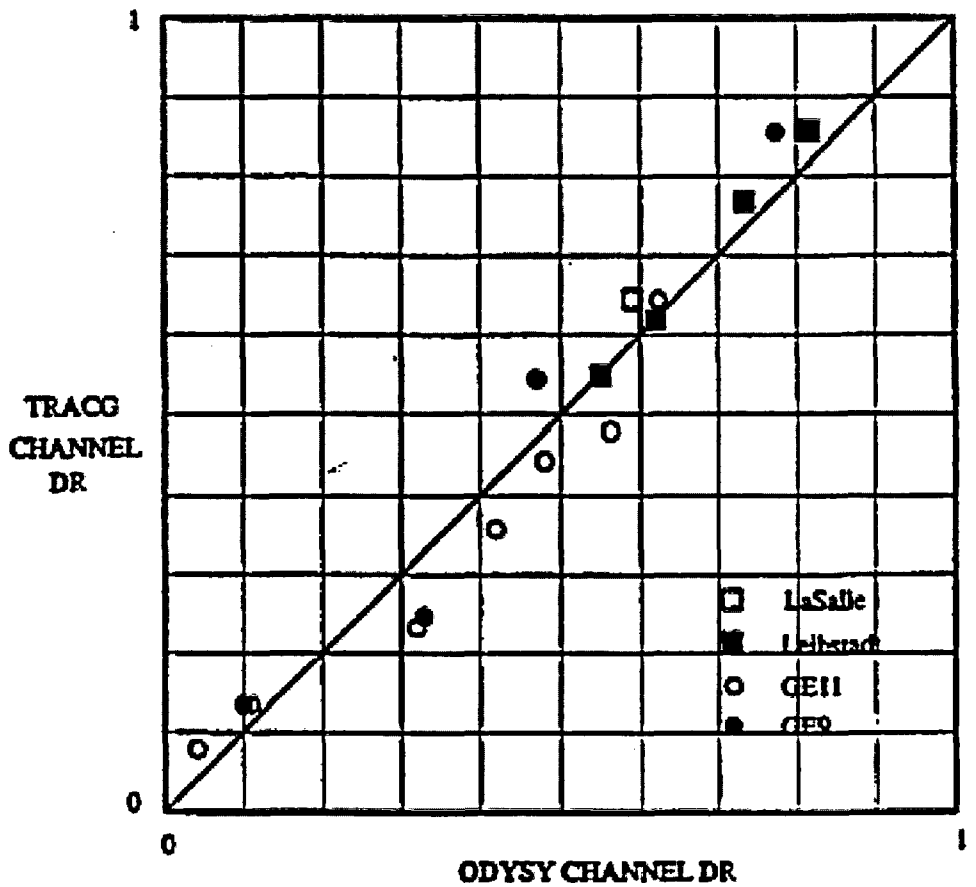

Figure 4.1d-2 TRAGC Channel Decay Ratio vs. ODYSY Channel Decay Ratio

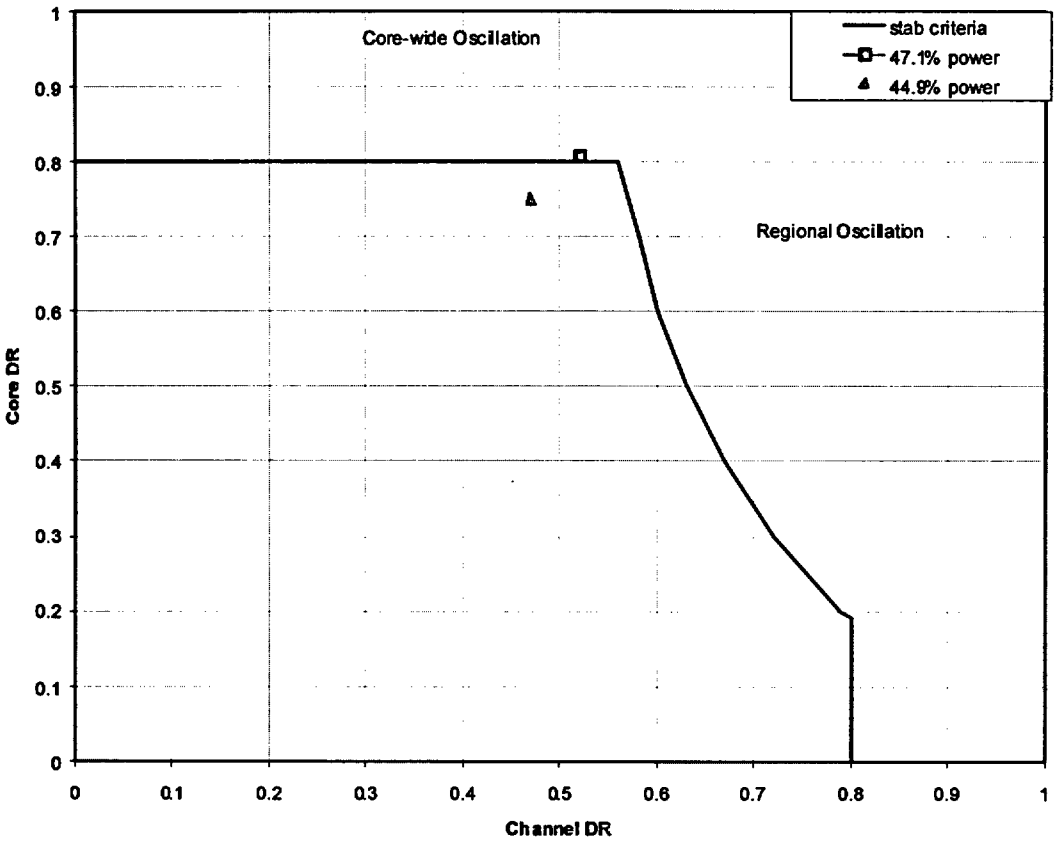

Figure 4.1d-3 NMP-2 Instability Event ODYSY Benchmark

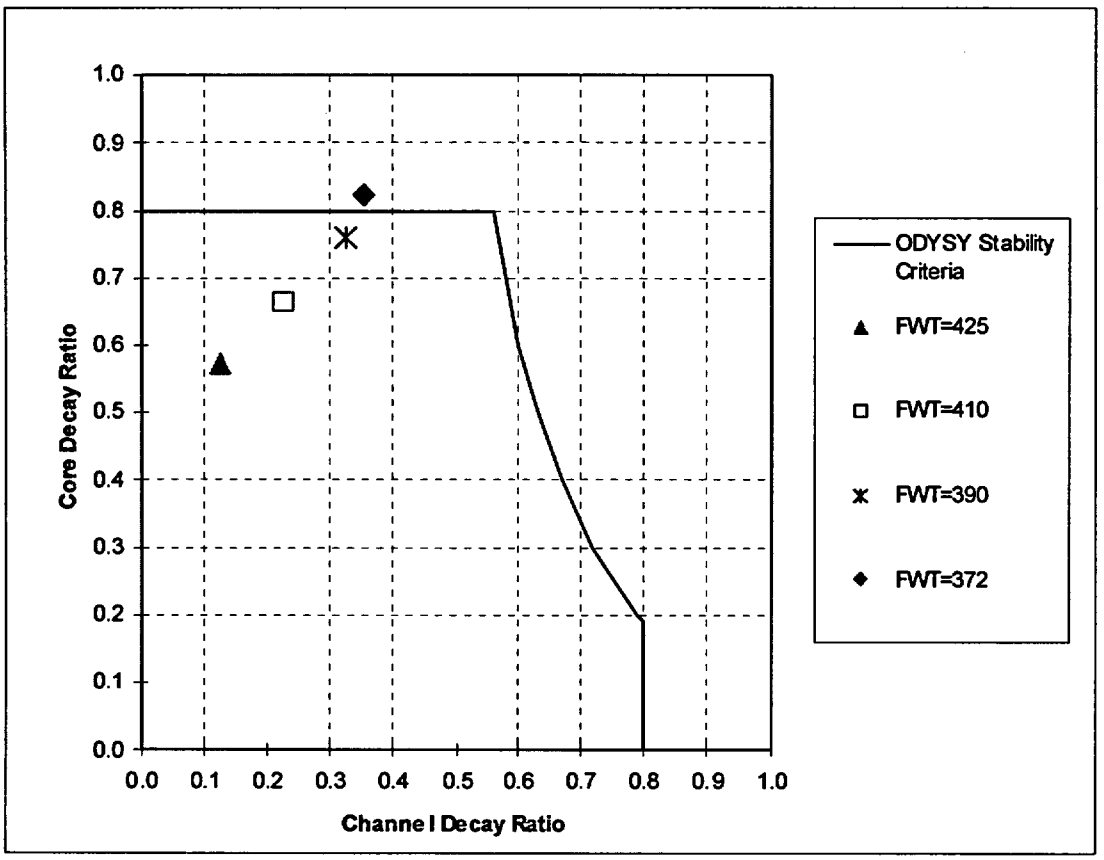

Figure 4.1d-4 Perry Instability Event ODYSY Benchmark: 425°F @ 47.4% power; 410°F @ 49.8% power; 390°F @ 52.2% power; 372°F @ 54.2% power

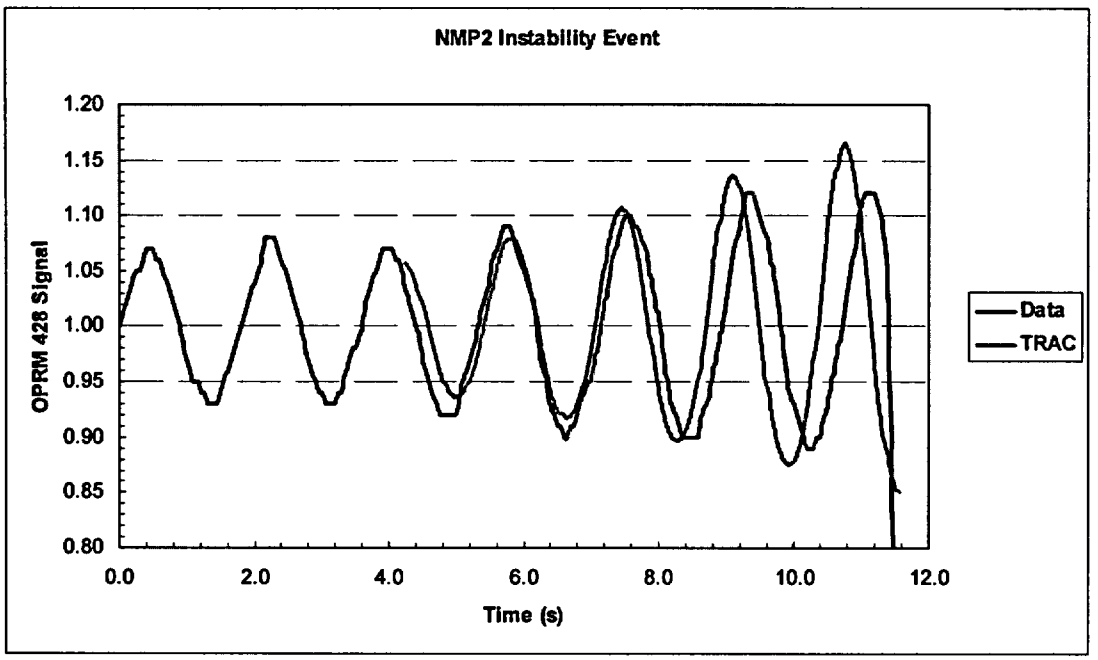

Figure 4.1d-5 NMP-2 Instability Event TRACG Benchmark

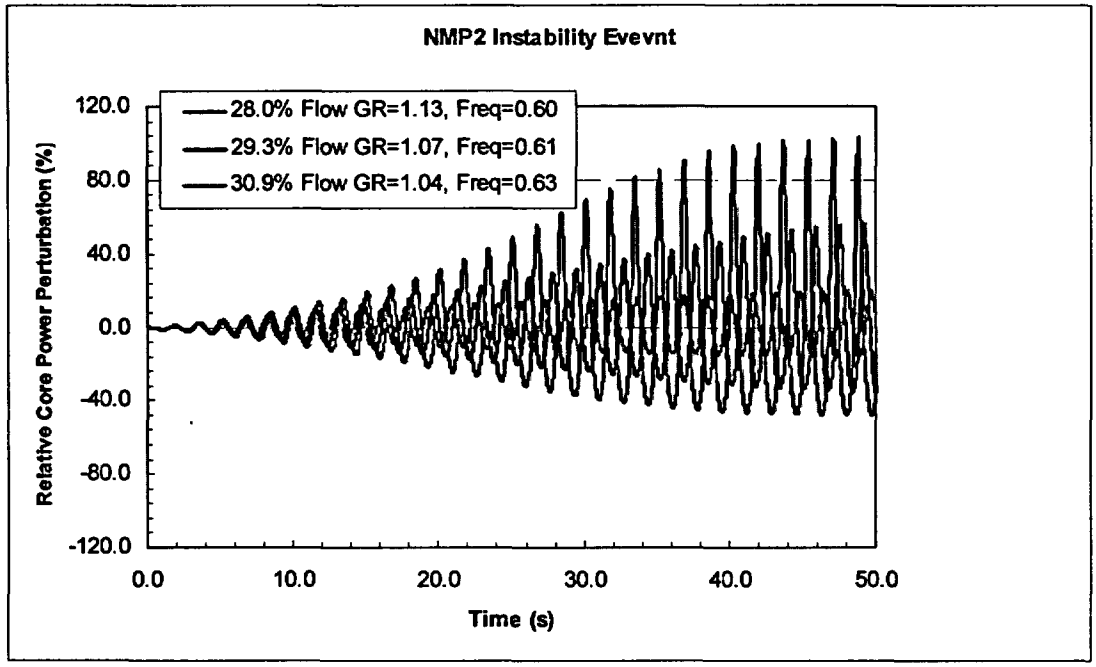

Figure 4.1d-6 NMP-2 Instability Event TRACG Flow Sensitivity

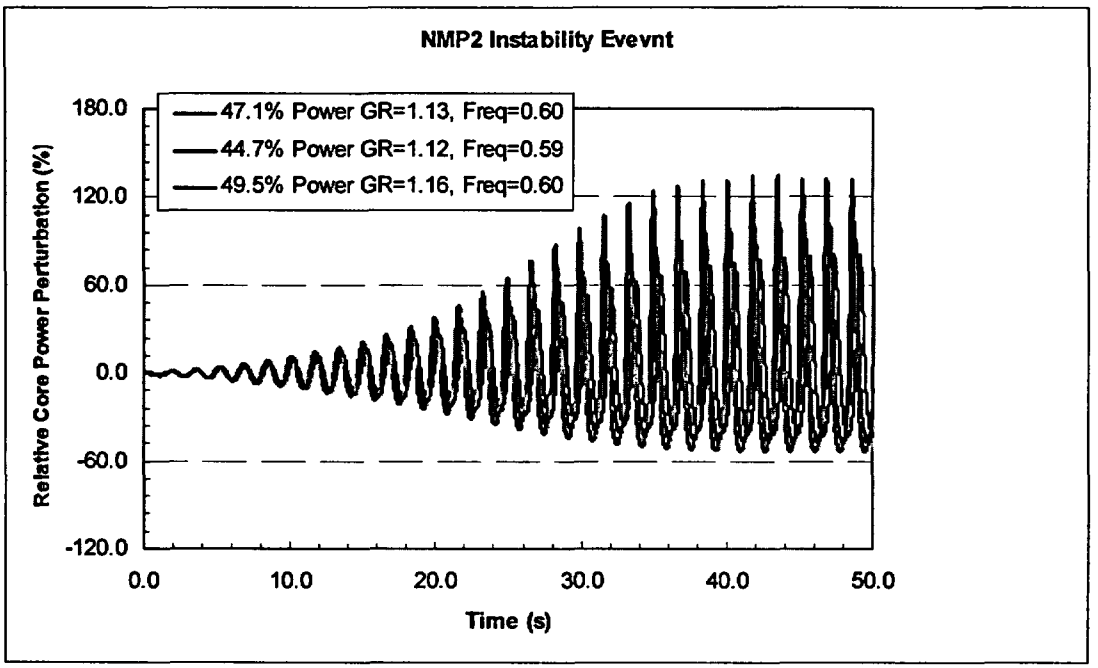

Figure 4.1d-7 NMP-2 Instability Event TRACG Power Sensitivity

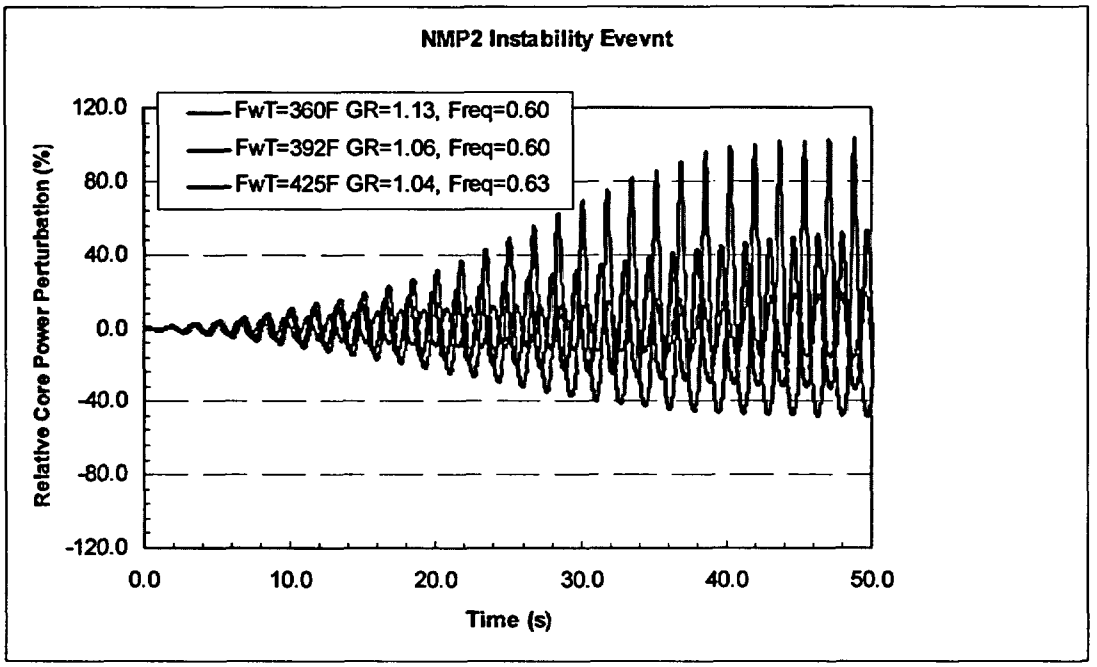

Figure 4.1d-8 NMP-2 Instability Event TRACG Feedwater Temperature Sensitivity

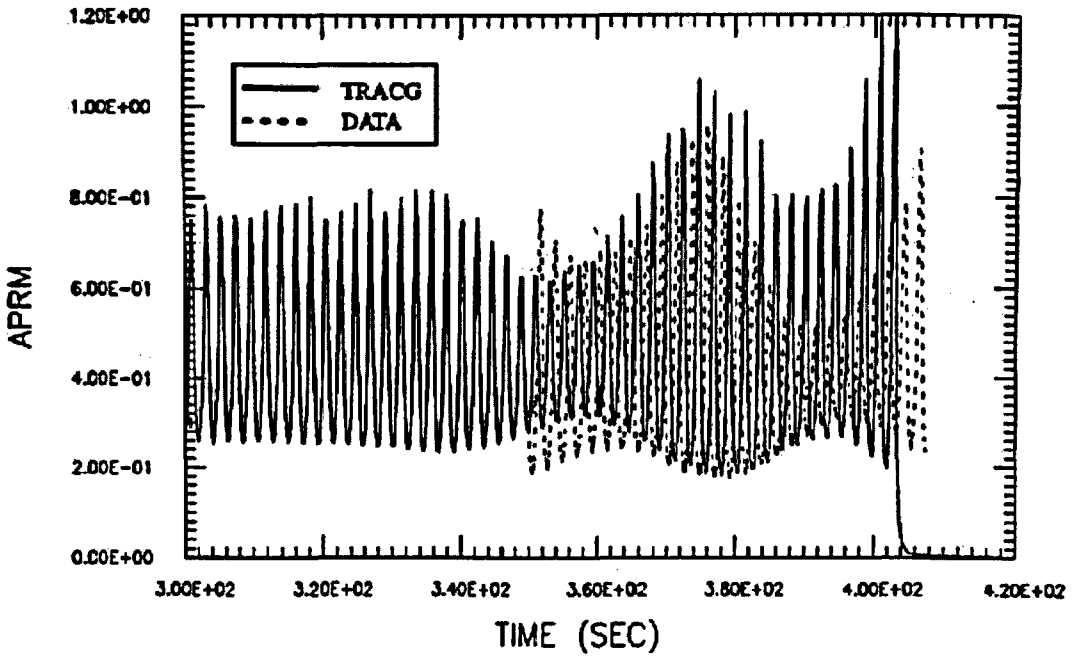

Figure 4.1d-9 (NEDE-32177P Rev 2 Figure 7.4-10) LaSalle Event Detailed APRM Comparison

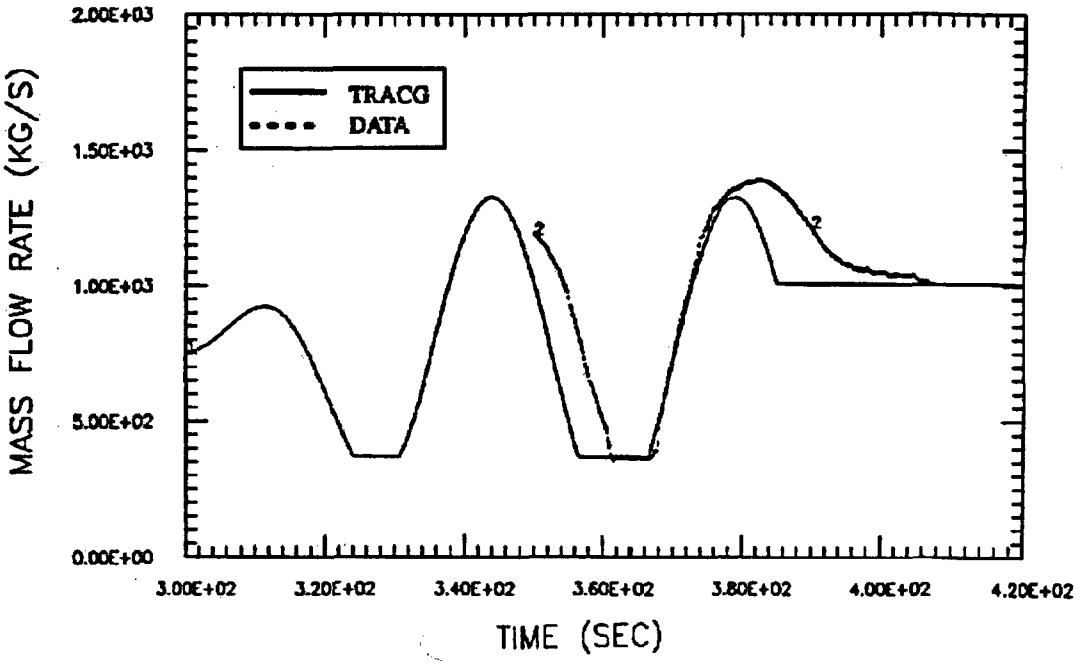

Figure 4.1d-10 **(NEDE-32177P Rev 2 Figure 7.4-11) LaSalle Event Detailed Feedwater Flow Comparison**

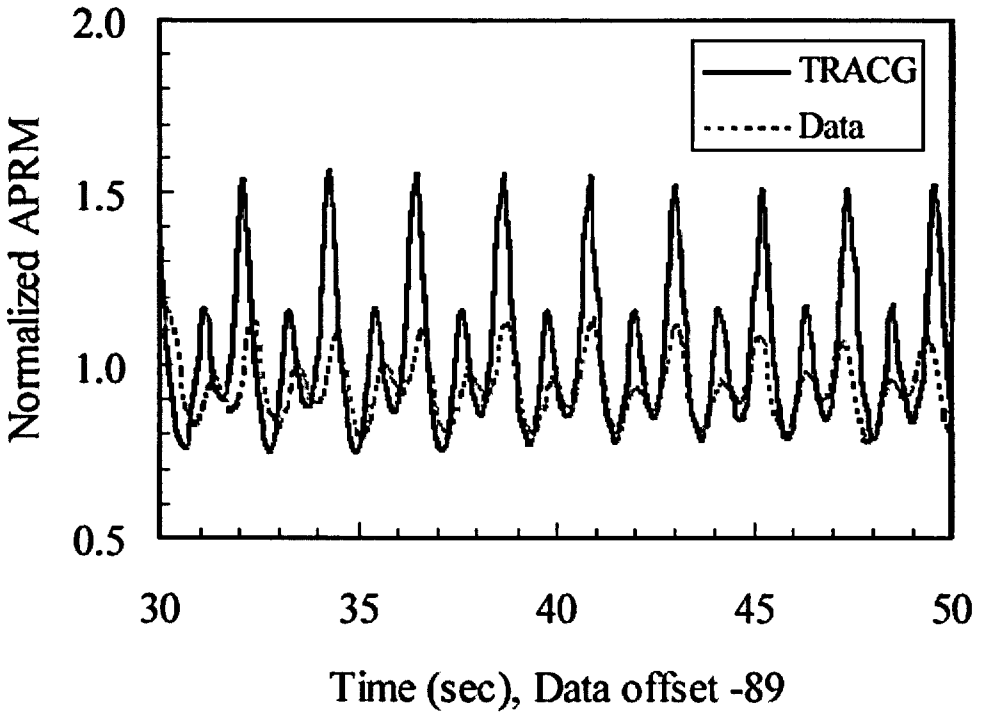

Figure 4.1d-11 **(NEDE-32177P Rev 2 Figure 7.7-7) Cofrentes Event Detailed APRM Comparison**

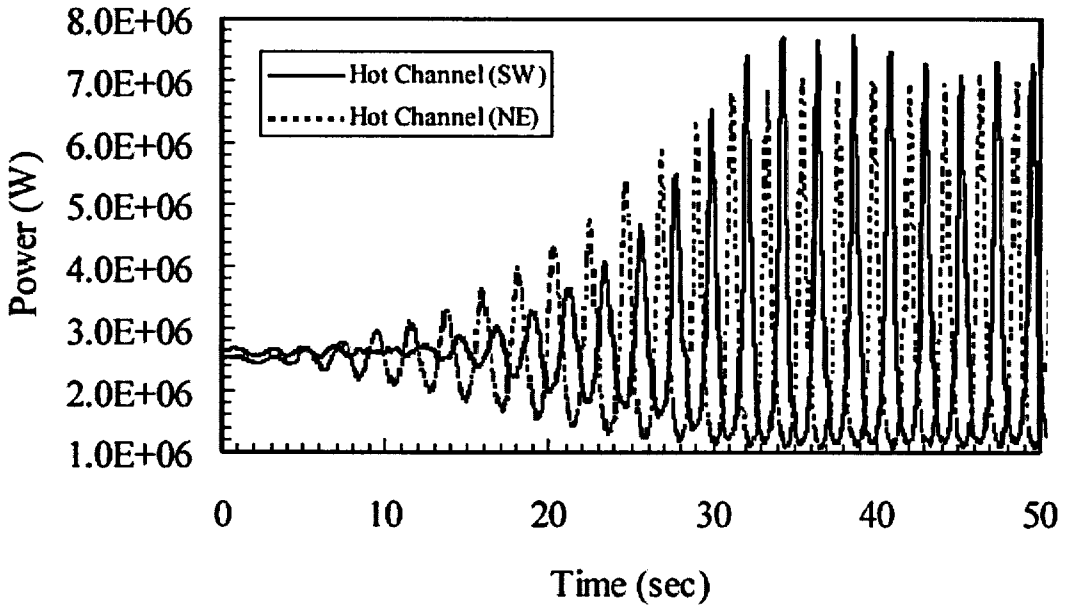

Figure 4.1d-12 **(NEDE-32177P Rev 2 Figure 7.7-8) Cofrentes Event Channel Power Response**

NRC RAI 4.1(e)
What is the impact on stability of void fraction histories less than 40%?

GE Response
[[

]]

NRC RAI 4.2
Address the impact of the 40 percent depletion assumption on the ATWS response.

GE Response
The 40% void depletion assumption can affect the void coefficient. The effect of void coefficient uncertainty has been addressed in previous studies. With respect to ATWS Overpressure results, uncertainty screening was performed in NEDE-32906P Supplement 1-A (MFN 03-148, November 26, 2003). The initial conditions for this study were for a plant at 113% of original rated power and 73% core flow, which are MELLLA+ type of conditions.

For an ATWS event, the steam line isolation causes a rapid increase in reactor vessel pressure, which results in core void reduction. Consequently, power increases with positive void reactivity insertion. For ATWS simulation purposes, the expected MSIV position and high flux scrams do not occur. The power excursion is initially mitigated by void production from the increased core heat flux, as well as negative doppler reactivity from increasing fuel temperature. Soon after the time the MSIVs are fully closed, Recirculation Pump Trip (RPT) is initiated on high pressure, such that core flow begins to decrease. At about this same time, the Safety/Relief Valves (S/RVs) open, reducing the rate of pressure increase. As core flow continues to decrease, core voiding increases, causing the power to decrease in parallel. Finally, the steam production decreases to the point at which the S/RV capacity is sufficient to relieve all of the steam generation, and the pressure begins to fall. Figures 4.2a and 4.2b show the response of key parameters for this event. These figures also contain the results for the void coefficient perturbation.

Analyses have been performed at +/- 1σ level for each of the model uncertainties. The results of the screening are shown in Figure 4.2c.

The analysis results show that the peak pressure results are [[

]]

Analyses have also been performed for another EPU plant with ODYN with a core-wide [[ ]] increase in ODYN void coefficient magnitude. The results are presented in Table 4.2a for BOC and EOC conditions. [[

]]

In addition, the effect on the peak pool temperature response is also addressed. Sensitivity studies have been performed with a core-wide [[ ]] increase in the ODYN void coefficient magnitude. A sensitivity study was performed for a limiting Pressure Regulator Failue – Open (PRFO) at both BOC and EOC exposure conditions. The results shown in Table 4.2b below show that the peak pool temperature is [[

]].

Table 4.2a ODYN Peak Vessel Pressure Void Coefficient Study

Event and Description	Exposure	Peak Vessel Pressure (psig)
PRFO Base Case	BOC	[[
PRFO with 10% void coefficient increase	BOC	
PRFO Base Case	EOC	
PRFO with 10% void coefficient increase	EOC	]]

Table 4.2b Suppression Pool Peak Temperature Void Coefficient Study

Event and Description	Exposure	Peak Suppression Pool Temperature (°F)
PRFO Base Case	BOC	[[
PRFO with 10% void coefficient increase	BOC	
PRFO Base Case	EOC	
PRFO with 10% void coefficient increase	EOC	]]

[[

]]

Figure 4.2a TRACG Power and Flow Response for MSIVC Event

[[

Figure 4.2b TRACG Pressure and Relief Valve Response for MSIVC Event

]]

[[

]]

Figure 4.2c MSIVC ATWS Peak Vessel Pressure Sensitivity to Individual Uncertainties (Pcase-Pnominal [kPa]

NRC RAI 5.0 Void-Quality Correlation
NRC RAI 5-1
Figure 2-2 of NEDC-33173P shows a plot of the typical void quality relation at high power/flow ratio. Evaluate the database supporting the void fraction correlation and plot the supporting validation measurement data on Figure 2-2. Identify the type of validation data on the plot, including the supporting tests types and the associated thermal-hydraulic conditions.

GE Response
The database for the Findlay Dix Correlation is described in the response to VY RAI 69 and further details are contained in the Reference 5-1 and in Attachment A to Reference 5-7.

As described in NEDE-21565, the 713 series of data were primarily used in the development of the correlation while other test series such as the 813 series were used for validation. The void-quality relation shown in Figure 2-2 is based on a calculation for a typical modern fuel bundle with a mass flux of 0.8 Mlb/ft^2-hr. This mass flux corresponds to a Reynolds number of approximately 1.1E5 in the fully rodded region of the bundle. Comparing this calculation to the void fraction data used in the development of the Findlay-Dix correlation is not perfectly meaningful as the bundle geometry and test conditions are not identical. However, the Findlay-Dix correlation is primarily a function of the Reynolds number, quality and fluid properties, and data were obtained for a Reynolds number of approximately 1.1E5 for both the 713 and 813 series. These data have been added to Figure 5-1 and are shown below. This Figure allows a qualitative assessment of the correlation. Detailed quantitative comparisons of the Findlay-Dix correlation to the test data are contained in Reference 5-1.

There are no significant trend differences between the comparisons to the development and validation data.

[[

]]

Figure 5-1 Void Fraction versus Quality - Data and Calculation.

NRC RAI 5-2

The void fraction calculation affects both the accuracy of the physics and the thermal-hydraulic calculations used to perform the design bases safety analyses. The objective is to confirm the void-quality correlation applicability ranges and assess any changes in the uncertainty of the correlation and its impact on the operating limit MCPR. Justify why the void quality correlation and the assumed uncertainty in the correlation are applicable for modern fuel (e.g., part-length rods, mixing vanes) and high energy operating conditions.

GE Response

The void correlation is correlated as a function of Reynolds number, quality and fluid properties. Since the Reynolds number is a function of mass flux, hydraulic diameter and fluid properties, and the fluid properties are a function of pressure, the void correlation can also be correlated as a function of hydraulic diameter, mass flux, quality and pressure. The parameter ranges for the void fraction data used to develop the void fraction correlation are given in Table 5-1. It is seen from this table that the parameter ranges cover all GE fuel products and operating ranges.

- The range in hydraulic diameters in the data is [[ ]], which is much larger than the range of hydraulic diameters in the fuel designs. The hydraulic diameter in recent GE fuel products range from [[ ]] for 8X8 fuel to [[ ]] in the fully rodded region of 10X10 fuel. In the region above the part length rods, the hydraulic diameters range from [[ ]] for 10X10 fuel to [[ ]] for 9X9 fuel.

- The pressure range covers atmospheric pressure to twice normal operating pressure for a BWR.

- The mass flux in a BWR ranges from approximately 400 kg/m^2-sec at natural circulation to approximately 1350 kg/m^2-sec at rated core flow, and it is seen that the mass flux range in the data far exceeds this range.

- The void fraction range in the data is from [[ ]] for simple geometry data and from [[ ]] for rod bundle data, while a typical exit void fraction in BWR fuel ranges from [[ ]], for the average bundle, to approximately [[ ]] for a high power 10X10 fuel bundle such as GE14 under EPU conditions.

In summary, the database for the void correlation covers all fuel products including 10X10 fuel and all operating ranges including EPU conditions.

The GE void fraction correlation is described in detail in the approved Reference 5-3. The qualification documented in the approved Reference 5-4, where the void correlation was compared to [[ ]] data points from the most representative full-scale bundles, yielded a standard deviation of [[ ]] in the void fraction, while the qualification against the wider set of [[ ]] data points as documented in Reference 5-1, 5-5 and the approved Reference 5-7 yielded a standard deviation or [[ ]] in the void fraction (See Table 5-2).

A void fraction of [[ ]], a limiting estimate of a void fraction observed in a transient under MELLA+ and EPU conditions, is relatively high and typical of the conditions where boiling transition will occur in a BWR fuel bundle. Also, since the OLMCPR is determined such that boiling transition will not occur, it is highly unlikely that a void fraction of [[ ]] will be exceeded (e.g., perhaps momentarily during a transient) by any significant amount. Some aspects of void fraction and bundle power warrant a brief discussion. For illustrative purposes, consider a one-dimensional, steady state energy balance for a BWR fuel channel. It can be shown that the flow quality is

$$x(z) = \frac{h_{in} - h_f}{h_{fg}} + \frac{1}{\dot{m} h_{fg}} \int_0^z \dot{q}'(\xi) d\xi ,$$

where the definition of flow quality is given by

$$x = \frac{\dot{m}_g}{\dot{m}_f + \dot{m}_g}$$

The flow quality is a function of pressure (fluid properties), inlet flow rate and subcooling, and the heat addition rate. For the case of "z" equal to the exit elevation, the integral term essentially represents the channel power. The steady state exit quality is directly proportional to the integrated channel power.

Figure 5-1 shows a typical plot of the void-quality relationship for a flow typical of a high power/flow ratio fuel bundle for the entire range from zero to one. Recognizing the relationship between quality and channel power, the figure has two interesting points. First, the lower end of the quality range has a relatively steep slope. Small power changes in this lower quality range correspond to a relatively large void fraction change. This behavior has implications relative to the impact of the void coefficient. In general, the void coefficient becomes more negative with increasing (average) void fraction. However, the net power effect considering the void-quality behavior is that in general, core power response is more strongly influenced by regions of the core with lower void fraction. In other words, the quantity $\Delta\alpha$; $\left(\partial\alpha/\partial P\right)\Delta P$ (P is power) tends to be larger at low void fraction, so that the feedback $\Delta k/k$; $1/k\left(\partial k/\partial\alpha\right)\Delta\alpha$ tends to be larger. Second, the higher quality (or power range) is relatively flat with respect to void fraction. Changes in power at high power result in relatively small void fraction changes. Also, in terms of core power response, net void feedback tends to be milder at higher void fractions.

It should be recognized that a BWR fuel bundle is designed and operated such that boiling transition will not occur during steady-state or abnormal operational occurrences, and, therefore, high void fractions, i.e., higher than [[ ]], will not occur. Figure 5-1 illustrates this point, noting that less than half of the quality range (X < 0.5) covers up to 90% void fraction. A significant power increase (or a factor of 2 change in quality) is required to drive the void fraction from 90 to 100%. It would require a bundle power of approximately [[ ]] for a bundle at rated flow to reach a void fraction of [[ ]], while in reality a high power fuel bundle operates at approximately [[ ]].

For high void fractions, the void quality correlation is based on sound physical principles, and accurately extrapolates the measured data to a void fraction of 1.0. Using the Zuber-Findlay expression for two-phase flow, the void fraction α can be expressed as

$$\alpha = \frac{j_g}{C_0 j + \overline{v_{gj}}}$$

Where:

C_0	=	distribution parameter
$\overline{v_{gj}}$	=	drift velocity
j_g	=	volumetric flux of steam vapor
j	=	volumetric flux of the mixture

The drift velocity is the difference in velocity between the vapor and the mixture volumetric flux. Generally the vapor phase velocity is greater because of buoyant forces. At high quality, the annular flow regime predominates. In the annular flow regime the liquid phase surrounds the fuel rods and channel. Locally $v_g = j + v_{gj}$. When substituting $j = \alpha v_g + (1-\alpha) v_l$ into this equation one get $v_{gj} = (1-\alpha) v_R$, where v_R is the local relative velocity. From this expression, it follows that $\overline{v_{gj}}$ must approach 0.0 at the limit of $\alpha = 1.0$. It can similarly be shown that C_o must approach 1.0 at the limit of $\alpha = 1.0$. In the GE void correlation, the drift velocity is characterized as:

$$\overline{V_{gj}} \propto (1-\alpha)$$

This characterization is applied over the entire annular flow regime, or for void fractions greater than about 0.7. For high void fractions and small values of $\overline{V_{gj}}$, the void fraction is dominated by the ratio of vapor mass flux to total mass flux, determined by a simple mass and energy balance for each node. The outstanding agreement over the entire range shown in the qualification [5-1] and illustrated in the response to RAI 5-1 validates this simple model for the drift flux. An extrapolation based on this model to void fractions all the way from 0.98 (the upper end of the data base) to pure steam flow is therefore justified. In summary, the GE void correlation is based on test data and covers a broad range of conditions. The correlation supports the full range of conditions expected during BWR operation, including CPPU, EPU and MELLLA+ conditions.

The part length rod (PLR) is the major new feature in current fuel products. The impact of PLRs has been investigated for a 4X4 bundle for a pressure of 1 MPa and more recently for an 8X8 bundle at rated BWR pressure of 7.2 MPa [5-7]. A small increase, approximately [[ ]], was observed in void fraction downstream of the PLRs compared to the case with no PLR (See Figure 5-2) for the low-pressure 4X4 data. The recent more representative 8X8 data taken at normal operating pressure shows a small increase, on the order of [[

]].

The void correlation has been implemented into the GE design codes such as PANACEA/ODYN/ISCOR/TASC and the correct implementation of the void correlation has been tested by functional testing. Therefore, the qualification of the void correlation applies for all design codes except TRACG. TRACG [5-6] has been separately compared to a set of the same data discussed above and yielded a standard deviation of [[ ]] in the void fraction.

Table 5-1 Void Fraction Correlation Database.

Data Source	Geometry	Hydraulic Diameter (m)	Pressure (MPa)	Mass Flux (kg/m^2-sec)	Inlet subcooling (K)	Exit quality (Max.)	Max void fraction
Simple Geometry	Tube or Annulus	[[					
CISE	[[						
ASEA-513							
GE							
ASEA-713							
ASEA-813	]]						]]

Table 5-2 Comparison Between Void Correlation and Database (Taken from References 5-5 and 5-7)

Data Source	Data Points (N)	Average Error $\overline{\Delta\alpha} = \overline{\alpha_m - \alpha_c}$	Standard Deviation $\sigma_{\Delta\alpha}$
CISE	[[ ]]	[[ ]]	[[ ]]
GE	[[ ]]	[[ ]]	[[ ]]
ASEA-713	[[ ]]	[[ ]]	[[ ]
Subtotal	[[ ]]	[[ ]]	[[ ]
ASEA-813	[[ ]]	[[ ]]	[[ ]]
ASEA-513	[[ ]]	[[ ]]	[[ ]]
TOTAL	[[ ]]	[[ ]]	[[ ]]

[[

]]

Figure 5-2 4X4 Void fraction Data – Sensitivity to PLR

[[

]]

Figure 5-3 8x8 Void Fraction Data – Sensitivity to PLR for Low Flow

[[

]]

Figure 5-4 8x8 Void Fraction Data Sensitivity to PLR for High Flow

NRC RAI 5-3

The LTR references relevant plots and information provided in the Vermont Yankee (VY) RAIs. Include the relevant discussion and plots in this LTR.

GE Response

Please see the Response to RAI 6.1, which was issued in GE Letter MFN 06-195, dated June 23, 2006.

NRC RAI 5-4
Provide a summary of how the void-quality correlation uncertainties are accounted for in the model uncertainties for the codes and the analytical methodologies used to perform the licensing bases safety analyses

GE Response
The impact of Void Fraction Uncertainties is summarized below for each of the major methods categories:

SLMCPR The MCPR Safety Limit is governed by uncertainties in quantities that influence the boiling transition process, namely thermal hydraulic and power distribution conditions. The SLMCPR is based on uncertainties in the Core Monitoring System. The monitoring system is based on a best estimate calculation with PANACEA and is used to monitor that the design limits, such as the OLMCPR, are not exceeded. The PANACEA power distribution uncertainties are based on a coupled nuclear thermal hydraulic evaluation. The nodal and radial power distribution uncertainties are determined directly from comparisons of PANACEA and TIP response from operating plants. Gamma scan data are also used to establish the power distribution accuracy directly. The result is a power distribution uncertainty that includes any void fraction uncertainty together with nuclear model uncertainties. The SLMCPR also includes uncertainties in the R-factor, which is a function of local pin power peaking. The sensitivity of R-factor to channel void fraction is discussed in detail in the response to RAIs 31 and 31-1 of Reference 5-11. This response, included as Attachment 1 to Enclosure 1, shows a net OLMCPR change of less than 1% for a change of 20% in bundle void fraction. Thermal hydraulic conditions such as pressure drop can also be influence by void fraction. The pressure drop correlations are developed under prototypical conditions along with the critical power correlation. Since the void fraction is included in the comparisons with pressure drop data, the void fraction effect is included in the pressure drop uncertainties. The SLMCPR model includes thermal hydraulic model uncertainties as described in Reference 5-7.

OLMCPR The effect of void fraction uncertainty on the transient ΔCPR and the OLMCPR is included in the transient model uncertainty. The model uncertainty is traditionally determined from comparisons plant transient tests and verified by model perturbations. The details of the transient model uncertainties are documented in References 5-4, 5-5 and 5-6. The TRACG uncertainty includes an explicit void coefficient component in its statistical uncertainty model.

Fuel Rod thermal Mechanical (LHGR) Similar to the SLMCPR, the majority of the power distribution uncertainty is determined by direct power distribution measurements and therefore includes void fraction uncertainties. However the local pin peaking uncertainty is determined from model calculations and therefore has a void coefficient component. The peak pin power in a typical fuel bundle is a weak function of void fraction, changing about 3% over a span from 0% void to 40% void and another 4% from 40% void to 70% void. Assuming a 3% uncertainty in void fraction at any one axial height, the void fraction contributes about 0.3% to the overall peak pin power uncertainty. This void uncertainty, when statistically combined with the other pin peaking uncertainties results in a negligibly small component of the overall peaking uncertainty.

Cold Shutdown Margin (SDM) The cold shutdown model does not directly depend on the void fraction model since it is analyzed at 0% voids. It indirectly depends on the void model because the exposure distribution depends on the void model used while the reactor is at power. Like the power distribution uncertainty, the shutdown margin uncertainty is determined directly by measurement and therefore includes any void model uncertainty in the PANACEA 3-D simulator.

LOCA Related Nodal Power Limits Nodal power limits and associated uncertainties are based on direct nodal power measurements taken from TIP and LPRM responses, which include any void distribution effects. The uncertainties are included in the determination of the upper bound peak cladding temperature (PCT). The conservatism of the licensing basis PCT is guaranteed by the conservative inputs required by 10 CFR 50 Appendix K. The licensing basis PCT has been shown to be more conservative than the upper bound PCT [Reference 5-10]

Stability In addition to other transient and steady state uncertainties discussed above, the void fraction influences the total steam volume and feedback under low flow conditions. The void fraction uncertainties are reflected in the overall transient model uncertainties, similar to those employed for determination of the OLMCPR uncertainties. For plants using an exclusion region, the void fraction uncertainty is included through the use of conservative inputs and the 0.2 margin that is applied to the decay ratio. For plants using a detect and suppress methodology, the set points are determined such the SLMCPR will not be violated, and the void fraction uncertainty are covered by the power distribution uncertainties included in the SLMCPR determination.

References

5-1 J. A. Findlay and G. E. Dix, BWR Void Fraction and Data, NEDE-21565, January 1977. General Electric Proprietary Information.

5-2 N. Zuber and J. A. Findlay, Average Volumetric Concentration in Two-Phase Flow Systems, ASME J. Heat Transfer, November 1965.

5-3 TASC-03A, A Computer Program for Transient Analysis of a Single Channel, NEDC-32084P-A, Revision 2, July 2002.

5-4 Letter, J. S. Charnley (GE) to H. N. Berkow (NRC), Revised Supplementary Information Regarding Amendment 11 to GE Licensing Topical Report NEDE-24011-P-A, MFN-003-086, January 16, 1986.

5-5 Letter, G. Stramback (GE) to NRC, Completion of Responses to MELLLA Plus AOO RAIs (TAC No. MB6157), MFN 04-026, March 4, 2004.

5-6 TRACG Application for Anticipated Operational Occurrences (AOO) transient Analyses, NEDE-32906P-A, Revision 1, April 2003.

5-7 Methodology and Uncertainties for Safety Limit MCPR Evaluations, NEDC-32601P-A, August 1999.

5-8 Power Distribution Uncertainties for Safety Limit MCPR Evaluation, NEDC-32694P-A, August 1999.

5-9 Applicability of GE Methods to Expanded Operating Domain, NEDC-33173P, February 2006.

5-11 GESTR-LOCA and SAFER Models for Evaluation of Loss-of-Coolant Accident, Volume III, Supplement 1, Additional Information for Upper Bound PCT Calculation, NEDE-23785P-A, Supplement 1, Revision 1, March 2002.

5-11 MFN-05-031, Letter to Louis Quintana, "REQUEST FOR ADDITIONAL INFORMATION – LICENSING TOPICAL REPORT NEDC-33006P, REVISION 1 "GENERAL ELECTRIC BOILING WATER REACTOR MAXIMUM EXTENDED LOAD LINE LIMIT ANALYSIS PLUS (MELLA+)" (TAC NO. MB6157)" April 11, 2005

NRC RAI 6.0 Process

GE Response
The changes to the LTR proposed by the RAI 6 responses are reflected in Enclosure 3 and shown by revisions bars. The LTR will be formally issued, reflecting these and other required changes, approximately 2 weeks after the closure of the methods related RAIs supporting the review of Tennessee's Valley Authority's license change request for an extended power uprate.

NRC RAI 6.1
The LTR summarizes the content of the VY RAIs. However, this eliminates relevant figures and evaluations. For the void fraction correlation, void reactivity coefficient, and Option 1D include the relevant figures and discussions so that the supporting information is integrated in this LTR.

GE Response
The relevant figures, tables, and discussion from the VY RAIs have been incorporated into the body of the LTR. Appropriate references have also been included.

NRC RAI 6.2
Appendix A contains many RAIs not related to the methods review. All EPU SRXB-A RAIs were cited in Appendix A. Many of these RAIs, did not address nor are they relevant to the Methods review. This array of RAIs hampers efficient use of the reference material. Delete the SRXB-A RAIs that were not part of the methods review.

GE Response
The table in Appendix A will be reduced to include only the VY RAIs that are related to the methods review.

In addition, because the VY RAIs in Appendix B are grouped and formatted according to the VY Supplemental submittals, the removal of individual RAIs would result in the section being fragmented and difficult to follow. GE believes that Appendix B is no longer an essential part of the Interim Methods LTR and, therefore, proposes its removal.

See Enclosure 3 for the revised Appendix A.

NRC RAI 6.3

Vermont Yankee SRXB-A Figures 6-1 thru 6-6 show the maximum bundle operating conditions of high density and EPU plants. Each plant specific application should, include the plant-specific data in the plots containing the high density and EPU plants maximum bundle operating conditions (Attachment 3, BVY 05-024)

(a) Therefore, include in the EPU applications the following bundle operating conditions with exposure in the EPU maximum bundle operating condition plots:
maximum bundle power,
maximum bundle power/flow ratio,
exit void fraction of maximum power bundle,
maximum channel exit void fraction,
peak linear heat generation rate and
peak end-of-cycle nodal exposure

(b) Provide quarter core map (assuming core symmetry) showing the bundle operating linear heat generation (MLHGR) and the minimum critical power ratio (MCPR) for beginning-of-cycle (BOC), middle-of-cycle (MOC) and end-of-cycle (EOC). Similarly, show the associated bundle powers.

GE Response

Section 4.3 of the Methods LTR will be modified, to specify that the requested core operating information be included with plant specific applications of the Methods LTR.

See Enclosure 3 for the revised Section 4.3.

ATTACHMENT 1 to ENCLOSURE 2

MFN 06-211

MELLLA+ RAI 31

Non-Proprietary Version

IMPORTANT NOTICE

This is a non-proprietary version of Attachment 1 to Enclosure 1 to MFN 06-211, which has the proprietary information removed. Portions of the Attachment to Enclosure 1 that have been removed are indicated by an open and closed bracket as shown here [[ ]].

MELLLA+ RAI 31

NRC RAI 31, R-Factor
The R-factor methodology is described in NEDC-32505P, "An R-Factor Calculation Method for GE11, GE12, and GE13 Fuel," dated July 1999. Evaluate the R-factor methodology to ensure that the key assumptions in the R-factor methodology remain applicable to the EPU/MELLLA+ conditions. Also evaluate the pin peaking factors used in the R-factor calculation for operation at high-void conditions. Amend the topical report accordingly, and amend the RAI responses for operation at the EPU/MELLLA+ conditions. RAIs 31-1 through 31-4 pertain to several features of the R-factor calculation, specifically the effects of the axial power shape, peaking distribution, exposure, and void fraction on the pin power peaking factor.

Response:
The R-factor is an input to the GEXL correlations which accounts for the effects of the fuel rod power distributions and the fuel assembly and channel geometry on the fuel assembly critical power. [[

]]

References

31-1 NEDC-32851P Rev.2,"GEXL14 Correlation for GE14 Fuel", Sept. 2001.
31-2 NEDC-32601P, "Methodology and Uncertainties for Safety Limit MCPR Evaluations",Dec.1996.

Table 31-1: Summary of Bundle 2 Results							
	R-factor	R-factor	R-factor	RIP	RIP	RIP	SLMCPR
	50%VF	70%VF	Difference	50%VF	70%VF	Difference	Difference
Exp			(70VF-50VF)			(70VF-50VF)	(Estimated)
[[							
							]]

[[

]]

[[

]]

[[

]]

NRC RAI 31-1

RAI 5 (Attachment B) and RAI 4 (Attachment D) of NEDC-32505P-A address the methods used to calculate the R-factor in terms of the axial power shape, peaking factors, local exposure, and void fraction. Provide updated responses to these RAIs. Explain the statement that the lattice peaking factors are weak functions of exposure and void and the relative rod power peaking factors ri are weak functions of the axial power shape, P(z).

GE Response

Response to Part 1

The R–factor calculation method for GE14 is essentially identical as the method described in NEDC-32050P-A for the GE12 product. The updated weighting parameters for GE14 have been provided in Reference 31-1. The change in the length of the PLRs is the only significant change in the generation of GE14 R-factors relative to the GE11, GE12, and GE13 process. The R-factor methodology for GE14 is given in Section 8 of Reference 31-1. The axial weighting shapes are defined and examples of the R-factor weighting process are given in Sections 8.2 through 8.5.

Response to Part 2

In NEDC-32505P-A, [[

]].